NAVAL POSTGRADUATE SCHOOL

MONTEREY, CALIFORNIA

THESIS

MISSION PLANNING OPTIMIZATION FOR INFANTRY OPERATIONS

by

Ryan A. Helm

June 2023

Thesis Advisor:	Ruriko Yoshida
Co-Advisor:	Ross J. Schuchard
Second Reader:	Christian R. Fitzpatrick

THIS PAGE INTENTIONALLY LEFT BLANK

REPORT DOCUMENTATION PAGE	*Form Approved OMB No. 0704-0188*

1. AGENCY USE ONLY *(Leave blank)*	**2. REPORT DATE** June 2023	**3. REPORT TYPE AND DATES COVERED** Master's thesis

4. TITLE AND SUBTITLE
MISSION PLANNING OPTIMIZATION FOR INFANTRY OPERATIONS

5. FUNDING NUMBERS

6. AUTHOR(S) Ryan A. Helm

7. PERFORMING ORGANIZATION NAME(S) AND ADDRESS(ES)
Naval Postgraduate School
Monterey, CA 93943-5000

8. PERFORMING ORGANIZATION REPORT NUMBER

9. SPONSORING / MONITORING AGENCY NAME(S) AND ADDRESS(ES)
N/A

10. SPONSORING / MONITORING AGENCY REPORT NUMBER

11. SUPPLEMENTARY NOTES The views expressed in this thesis are those of the author and do not reflect the official policy or position of the Department of Defense or the U.S. Government.

12a. DISTRIBUTION / AVAILABILITY STATEMENT
Approved for public release. Distribution is unlimited.

12b. DISTRIBUTION CODE
A

13. ABSTRACT (maximum 200 words)

Geospatial intelligence is readily available to tactical-level leaders for mission planning, but few analytical models exist or are directly available for exploitation by end-users. This capability gap results in a slower planning process that decreases in comprehensibility and precision as time and support available are constrained. We offer a capability to fill this gap in offensive operations by formulating four models for: helicopter landing zone detection, tactical pathfinding, battlespace geometry optimization, and course of action selection optimization. Methods leveraged include geospatial data analysis, unsupervised machine learning, multi-objective minimum-cost flow, and weighted-sum multi-objective optimization. In our experiment, we run our models to generate courses of action for an air assault at Camp Pendleton, California. By choice of landing zone, route, supporting machine gun position, and objective entry point, the model finds 785,664 possible decision combinations for this scenario. The model constrains to 220 courses of action by user preferences and doctrinal considerations. The decision-maker is presented with a preferred number of optimal courses of action after evaluating the set of branch plans with a multi-objective optimization. This research demonstrates the utility for analytic models to rapidly and precisely inform decision-making cycles at the tactical edge.

14. SUBJECT TERMS
multi-objective optimization, terrain analysis, geospatial analysis, decision aid, tactical pathfinding, helicopter landing zone, battlespace geometries, course of action optimization, unsupervised machine learning, clustering, minimum-cost flow

15. NUMBER OF PAGES
109

16. PRICE CODE

17. SECURITY CLASSIFICATION OF REPORT	**18. SECURITY CLASSIFICATION OF THIS PAGE**	**19. SECURITY CLASSIFICATION OF ABSTRACT**	**20. LIMITATION OF ABSTRACT**
Unclassified	Unclassified	Unclassified	UU

NSN 7540-01-280-5500

Standard Form 298 (Rev. 2-89)
Prescribed by ANSI Std. 239-18

THIS PAGE INTENTIONALLY LEFT BLANK

Approved for public release. Distribution is unlimited.

MISSION PLANNING OPTIMIZATION FOR INFANTRY OPERATIONS

Ryan A. Helm
Captain, United States Marine Corps
BSISE, Ohio State University, 2017

Submitted in partial fulfillment of the
requirements for the degree of

MASTER OF SCIENCE IN OPERATIONS RESEARCH

from the

NAVAL POSTGRADUATE SCHOOL
June 2023

Approved by: Ruriko Yoshida
Advisor

Ross J. Schuchard
Co-Advisor

Christian R. Fitzpatrick
Second Reader

W. Matthew Carlyle
Chair, Department of Operations Research

THIS PAGE INTENTIONALLY LEFT BLANK

ABSTRACT

Geospatial intelligence is readily available to tactical-level leaders for mission planning, but few analytical models exist or are directly available for exploitation by end-users. This capability gap results in a slower planning process that decreases in comprehensibility and precision as time and support available are constrained. We offer a capability to fill this gap in offensive operations by formulating four models for: helicopter landing zone detection, tactical pathfinding, battlespace geometry optimization, and course of action selection optimization. Methods leveraged include geospatial data analysis, unsupervised machine learning, multi-objective minimum-cost flow, and weighted-sum multi-objective optimization. In our experiment, we run our models to generate courses of action for an air assault at Camp Pendleton, California. By choice of landing zone, route, supporting machine gun position, and objective entry point, the model finds 785,664 possible decision combinations for this scenario. The model constrains to 220 courses of action by user preferences and doctrinal considerations. The decision-maker is presented with a preferred number of optimal courses of action after evaluating the set of branch plans with a multi-objective optimization. This research demonstrates the utility for analytic models to rapidly and precisely inform decision-making cycles at the tactical edge.

THIS PAGE INTENTIONALLY LEFT BLANK

Table of Contents

List of Figures

List of Tables

THIS PAGE INTENTIONALLY LEFT BLANK

List of Acronyms and Abbreviations

3DEP	3D Elevation Program
AFC	assault force commander
AFL	assault flight leader
AFRL	Air Force Research Laboratory
AMC	air mission commander
AO	area of operations
API	application programming interface
ATAK	Android Tactical Assault Kit
C2	command and control
CivTAK	Civilian Team Awareness Kit for Android
COA	course of action
CRS	coordinate reference system
DEM	digital elevation model
DCGS	Distributed Common Ground System
DCGS-N	Distributed Common Ground System-Navy
DHS	Department of Homeland Security
DOD	Department of Defense
DSM	digital surface model
DT	distance transformation

EAB	expeditionary advanced bases
EMLCOA	enemy's most likely course of action
ESA	European Space Agency
FSP	fire support plan
GBASM	ground-based anti-ship missile
GEOINT	geospatial intelligence
GIS	geospatial information systems
GIST	geographic information support team
GOTS	government off-the-shelf
GTL	gun-target line
HLS	helicopter landing suitability
HLZ	helicopter landing zone
HOLF	Helicopter Outlying Airfield
ICOP	Intelligence Carry-On Program
IM	influence map
IOP	index of passibility
ISR	intelligence, surveillance, and reconnaissance
ISR/IO	intelligence, surveillance, and reconnaissance and information operations
KML	Keyhole Markup Language
LZ	landing zone
MAGTF	Marine Air-Ground Task Force
MCOO	modified combined obstacle overlay

MCPP	Marine Corps Planning Process
MCTP	Marine Corps Tactical Publication
MCWP	Marine Corps Warfighting Publication
MEF	Marine expeditionary force
MEU	Marine expeditionary unit
MOE	measures of effectiveness
MSL	minimum safe line
NATO	North Atlantic Treaty Organization
NGA	National Geospatial-Intelligence Agency
NIWC-PAC	Naval Information Warfare Center-Pacific
NTTP	Navy tactics, techniques, and procedures
PZ	pickup zone
R2P2	Rapid Response Planning Process
RMSE	root mean square error
SBF	support by fire
SDZ	surface danger zone
SMEs	subject matter experts
SOM	scheme of maneuver
SOPs	standard operating procedures
SPMAGTFs	Special Purpose Marine Air-Ground Task Forces
T/O	table of organization and equipment
TAK	Team Awareness Kit

TIGER	Topologically Integrated Geographic Encoding and Referencing
TRP	target reference point
UAV	unmanned aerial vehicle
UGR	unmanned ground robot
USGS	U.S. Geological Survey
USMC	U.S. Marine Corps
WEZ	weapon engagement zone

Executive Summary

Geospatial intelligence (GEOINT) is readily available to tactical-level leaders for mission planning, but few analytical models exist or are directly available for exploitation by end-users. This capability gap results in a slower planning process that decreases in comprehensibility and precision as time and support available are constrained. We offer a capability to fill this gap in offensive operations by formulating four models for: helicopter landing zone (HLZ) detection, tactical pathfinding, battlespace geometry optimization, and course of action (COA) selection optimization.

We analyze open-source geospatial data from Google Earth Engine with layers describing elevation, slope, land cover, and road use at a 10-meter resolution. Methods leveraged by our models include geospatial data analysis, unsupervised machine learning, multi-objective minimum-cost flow, and weighted-sum multi-objective optimization. Model outputs include quantifiable risk trade-off metrics to inform decision-makers. Resulting graphics and metadata are written to Keyhole Markup Language (KML) for interoperability with existing mission planning software and Google Earth on a wide variety platforms.

In our experiment, we run our models to generate COAs for an air assault at Camp Pendleton, California. By choice of HLZ, route, supporting machine gun position, and objective entry point, the model finds 785,664 possible decision combinations for this scenario. The model constrains to 220 COAs by user preferences and doctrinal considerations. The decision-maker is presented with a preferred number of optimal COAs after evaluating the set of branch plans with a multi-objective optimization.

This research demonstrates the utility for analytic models to rapidly and precisely inform decision-making cycles at the tactical edge. The research sponsor is currently developing implementations of these models for existing mission planning software, resulting in robust geospatial analysis models that will be available directly to small-unit leaders for mission planning support. Additional applications of these models are possible for expeditionary advanced base (EAB) operations, where the models may be applied to enumerate ground-based anti-ship missile (GBASM) firing points and route networks in the First and Second Island Chains.

THIS PAGE INTENTIONALLY LEFT BLANK

Acknowledgments

Among all of our nation's resources—economic, intellectual, and cultural—none are more precious than our nation's young enlisted Marines. For 247 years, selfless young men and women of our Corps have carried their duty into eternity in the name of freedom. This thesis is dedicated to the mothers, fathers, sisters, brothers, and spouses who bravely lend their loved ones to the Marine Corps in service of the United States of America. It is my hope that this research will contribute to putting our Marines in the most unfair fight possible—so that they may continue to win in combat and return home to their families and communities safely.

I am deeply grateful to my advising team, Professor Ruriko Yoshida and Lieutenant Colonel Ross Schuchard, for their mentorship, guidance, feedback, and patience as I freely explored the operational problems that captivated my curiosity and intellectual will. I am indebted and humbled by the efforts of my second reader, Christian Fitzpatrick, who tirelessly and enthusiastically pursued the near-term implementation of this thesis for use by warfighters in the fleet. I thank all faculty in the Operations Research Department who have given the incredible gift of education to my peers and me.

THIS PAGE INTENTIONALLY LEFT BLANK

CHAPTER 1:
Introduction

> In select cases, we will explore investments in decision support tools that leverage data science and artificial intelligence for the tactical commander. These smaller, high impact investments will facilitate experimentation to determine how it can assist our commanders in the field.
>
> —General David H. Berger (2019), *Commandant's Planning Guidance*

With modern sensing capabilities, vast quantities of geospatial intelligence (GEOINT) are collected for processing. Processing of GEOINT for mission planning purposes requires higher-echelon assets and capabilities that are not widely available to tactical-level leaders and planners. For example, a modified combined obstacle overlay (MCOO) is a very general product for GEOINT terrain analysis, but it is built at the Marine Air-Ground Task Force (MAGTF) level by the G-2 and G-3. Topographic platoons have very limited personnel to detach below the MAGTF level, and the terrain analysis capability of software fielded to small-unit leaders is limited to line-of-sight (viewshed) analysis. In this thesis, we propose data analysis and optimization models for specific mission planning purposes that are generalizable such that they may be fielded to small-unit leaders and commanders for direct use on existing hardware.

1.1 Problem Description

Warfare encompasses components of both art and science. In regard to resources available to leaders, there are few tools and data analysis models available to augment decision-making in the scientific realm of warfighting. Lethality and survivability can be improved with geospatial data analysis and optimization tools that increase the speed, comprehensibility, and precision with which tactical-level decisions are made. Without analysis tools, leaders still plan manually with laminated paper maps and protractors or with tablets to display digital map imagery and plots.

In this thesis, we model an offensive air assault for an airfield seizure of the Helicopter Outlying Airfield (HOLF), Camp Pendleton, California. We selected this region for the complex coastal terrain that may mirror an area of operations (AO) in the First and Second Island Chains. An air assault is similar to any general offensive maneuver, with the added choice of where friendly forces will be located to start the operation. This can make the direction of attack much more complex to consider and is further made challenging without the ability to perform physical reconnaissance on the terrain before the operation. There is added pressure for the assault force commander (AFC) in this scenario: planning must be conducted backwards beginning with the ground scheme of maneuver (SOM). The entire MAGTF must know a reasonably final ground SOM before beginning planning to support and conduct the air assault.

1.2 Models and Methods

> Planning involves elements of both art and science, combining analysis and calculation with intuition, inspiration, and creativity.
>
> —Marine Corps Warfighting Publication (MCWP) 5-10, Headquarters, Marine Corps (2015b)

To aid small-unit leaders and commanders with spatial analysis and calculation, we propose several models to exploit GEOINT during mission planning and execution. First, we develop a helicopter landing zone (HLZ) selection model. This model filters geospatial data to find regions suitable for HLZs, applies the k-means centroid clustering method to segment regions, and generates landing boxes from those decomposed regions.

Next, we develop a tactical pathfinding model for route selection. This model allows users to select relative risk assessments of terrain qualities, enemy fields of fire, and enemy observation. The model then returns the minimum-cost flow from the starting location to the ending location across a consolidated cost-grid of the AO generated from the weighted sums of the cost-assessed terrain.

For the third model, we develop a method for determining weapons employment positions by optimizing battlespace geometries relative to friendly and enemy positions. This is achieved

by analyzing the intersection of viewsheds from all desired targets. From the intersected region, we measure and plot descriptive data regarding the effectiveness of employment from each feasible position. Battlespace geometry outputs may be used as additional layers for the tactical pathfinding model when considering combinations of decisions.

Finally, we propose a model for air assault course of action (COA) generation and selection by choice of: HLZ, pathfinding risk tolerance, supporting weapons employment location, and objective entry location. We apply several tactical constraints and user inputs to constrain the feasible solution space, then individually evaluate each branch plan for its effectiveness. We apply a multi-objective optimization with user-selected importance weights to return a preferred number of desirable COAs.

1.3 Objective

The objective of our research is to provide useful decision-support models fieldable directly to tactical-level leaders on existing hardware. We achieve this by building models with intuitive inputs and outputs that mirror human decision-making factors and doctrine for each model's respective tasks. Resulting graphics and metadata are written to industry standard format for geospatial overlays, ensuring compatibility with existing tactical applications.

An additional objective of this thesis is to provide an adaptation of the HLZ generation model for deterrence analysis in the First and Second Island Chains. With modified parameters, the HLZ model is capable of enumerating discrete locations for firing points, resupply points, operations centers, and expeditionary advanced bases (EAB). A method for enumerating EAB locations is critical for force planning and is foundational for analysis with the application of stochastic and network models.

1.4 Thesis Organization

Chapter 2 contains general background information regarding military planning and intelligence operations related to this thesis, as well as a literature review. Chapter 3 describes the methodology for all four models. Chapter 4 contains the scenario application of our models and results. Chapter 5 summarizes our conclusions.

THIS PAGE INTENTIONALLY LEFT BLANK

CHAPTER 2:
Background

In Chapter 2, we provide an overview of context, applicability, and related work regarding the methodologies of this thesis. Section 2.1 introduces intelligence and information operations operating concepts and Department of Defense (DOD) efforts to build platforms for real-time intelligence processing and distribution. These platforms may be further leveraged as hosts for our models. Section 2.2 provides us with an overview of the four planning processes used by the U.S. Marine Corps (USMC), giving context on how our models enhance doctrinal planning. Section 2.3 expands on the Tactical Planning Process derived from the Troop Leading Steps, where we find the direct applicability for our models. Section 2.4 gives an overview of Air Assault planning, the example planning scenario for our model application. Section 2.5 reveals the current capability gaps that prevent small-unit leaders from exploiting GEOINT in this scenario. In Section 2.6, we provide background on existing research that may be applied or expanded upon to provide a direct capability to small-unit leaders for the analysis of GEOINT, increasing the effectiveness of doctrinal planning processes.

2.1 Intelligence, Surveillance, Reconnaissance, and Information Operations

> "Indeed, the National Geospatial-Intelligence Agency, a U.S. intelligence agency that currently has a total of 14,500 personnel, recently estimated that it would need more than 8 million people just to analyze all of the imagery of the globe that will be generated in the next twenty years."
>
> —Christian Brose (2020), *The Kill Chain*

The objective of intelligence is provide accurate, expedient, and pertinent knowledge about the enemy and the operating environment (Headquarters, Marine Corps 2018b). Intelligence supports a commander's decision making process by reducing uncertainty. While

uncertainty can never be eliminated, intelligence can validate assumptions and address key planning factors regarding the environment and general situation (Figure 2.1).

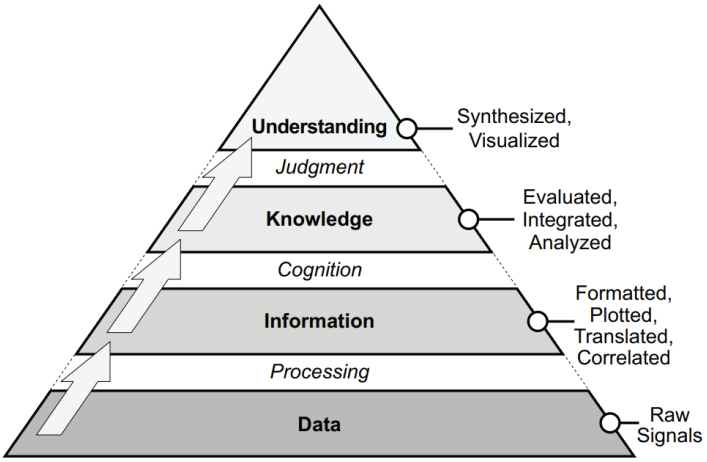

Figure 2.1. An information hierarchy describes the process of turning raw data into actionable intelligence for a decision-maker. In high volumes, raw data can increase uncertainty—it must be processed into applicable knowledge for a specific military decision. Source: Headquarters, Marine Corps (2018b).

Intelligence facilitates command and control and drives operational planning by providing context for decision-making. In support of operations, intelligence identifies opportunities and limitations in the situation, describes enemy strengths and critical vulnerabilities, and validates assumptions. Good intelligence is provided rapidly, allowing commanders to build and sustain operational tempo.

Timely intelligence delivery requires a real-time network for information planning, collection, processing, dissemination, and utilization (Figure 2.2). The Distributed Common Ground System (DCGS) is an example of one long-standing joint program developed to integrate multi-domain data collected from various sensors and platforms on a single system. Many DOD organizations and defense contractors contribute technologies that interface with and support the DCGS and intelligence, surveillance, and reconnaissance and information operations (ISR/IO), including the Naval Information Warfare Center-Pacific (NIWC-PAC).

NIWC-PAC develops systems supporting ISR/IO by combining adversarial observations with data collected from sea to space, distilling it into comprehensible and meaningful information for decision-makers.

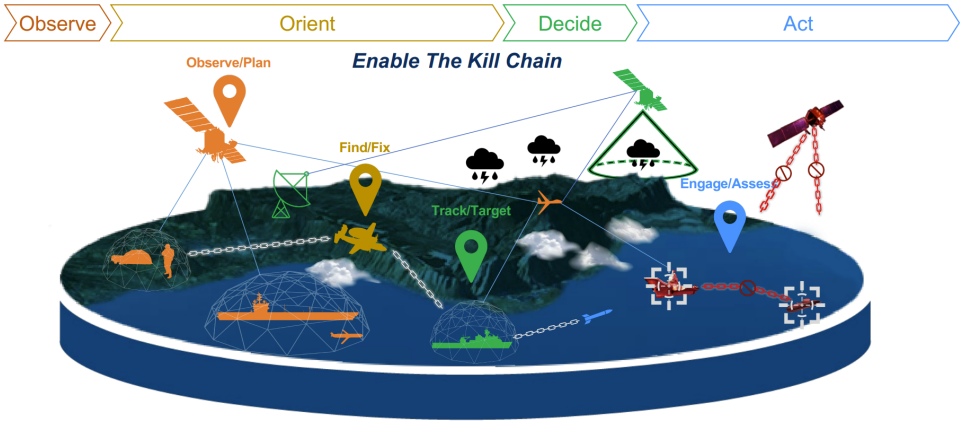

Figure 2.2. A commanders' ability to complete decision making cycles (observing, orienting, deciding, and acting) is key for success in warfare. ISR/IO systems provide timely information to decision-makers, allowing for faster, more comprehensive, and precise decision cycles. A quicker and more effective kill chain deters adversaries from a conflict they cannot win. Source: Hanaki (2022).

2.1.1 Platforms

Our models require platforms with access to GEOINT for analysis and user interface. The DCGS and its portable version, the Intelligence Carry-On Program (ICOP), provide networked platform solutions in command and control (C2) nodes. Android-based tactical tablets are available for small-unit leaders in distributed operations. Team Awareness Kit (TAK) provides the primary software for mission planning to the services, with available versions for all platforms. As described in Chapter 3, model output is designed to be interoperable with TAK products on all platforms.

Distributed Common Ground System

The Distributed Common Ground System-Navy (DCGS-N) is the Navy's primary system to network intelligence, surveillance, reconnaissance, targeting, processing, and exploitation (Tollefson 2021). The objective of DCGS-N is to combine and correlate intelligence in real-time, enhancing warfighter situational awareness. The ICOP is a variant of DCGS-N, available for expeditionary forces ashore.

Intelligence Carry-On Program

ICOP is a portable workstation that extends the intelligence, surveillance, and reconnaissance (ISR) Enterprise and DCGS-N capabilities for unit-level forces (Hanaki 2022). BAE Systems designed the workstation to provide the same exploitation of multi-domain intelligence data for enhancing the warfighter's common operational picture. According to NIWC-PAC's website, ICOP is capable of integrating data from airborne and organic sensors, compiling a multi-dimensional battlespace picture.

Aside from ISR and computing capabilities, the engineering and integration team leads claim the greatest benefit of ICOP is as a platform for continuous delivery of analysis and processing capabilities to the fleet, at a development and fielding speed that is relevant to warfighters who need them (Piedfort 2022). ICOP's experimentation and development cycle has high agility because the baseline and engineering teams are all-government, with complete control of hardware and software configurations (Piedfort 2022). This allows users to bypass the need for contractor support—critical for a responsive, efficient, and self-sufficient system.

Android Team Awareness Kit

The Civilian Team Awareness Kit for Android (CivTAK) is a government off-the-shelf (GOTS) software suite which provides geospatial information and shared situational awareness for users (TAK Product Center n.d.). Software engineers at the Air Force Research Laboratory (AFRL) developed CivTAK, along with numerous other inter-operable products in the TAK family. The TAK product variants are nearly identical, with additional specific features in each product that cater to the end-user. Base CivTAK features include (TAK Product Center n.d.):

- Very high-resolution imagery support;
- Collaborative mapping;
- Overlay manager;
- Elevation tools: heat maps, contour maps, and viewsheds;
- Geospatial measurement tools for range and bearing;
- Chat and file sharing;
- Casualty evacuation tool;
- 3D geospatial models;
- Driving and walking navigation;
- Precision targeting; and
- Video sharing and streaming.

The military variant of CivTAK is Android Tactical Assault Kit (ATAK). This variant includes additional features such as unmanned aerial vehicle (UAV) sensor integration and military radio compatibility. The TAK Product Center now maintains ATAK, which is currently in use by over 72,000 DOD, Department of Homeland Security (DHS), military, and non-federal users (Air Force Research Laboratory n.d.).

2.2 Overview of Planning Processes

> Effective decision-making requires both the situational understanding to recognize the essence of a given problem and the creative ability to devise a practical solution. Hence, an essential function of planning is to promote understanding of the problem—the difference between existing and desired conditions—and to devise ways to solve it.
>
> —MCWP 5-10, Headquarters, Marine Corps (2015b)

In Section 2.2, we explore several planning processes employed by the USMC. The four fundamental planning processes are the Marine Corps Planning Process (MCPP), Rapid Response Planning Process (R2P2), Joint Planning Process, and Troop Leading Steps (Headquarters, Marine Corps 2015b). We introduce MCPP and R2P2 as planning process frameworks that benefit from problem and COA analysis. Subsequently, we outline the Troop Leading Steps—the planning framework used at the small-unit level—which most directly describes the advantages provided by models in Chapter 3.

2.2.1 Marine Corps Planning Process

As described in MCWP 5-10, MCPP is a "proven, intellectually rigorous approach to planning." MCPP requires six steps involving problem framing, COA development, COA war game, COA comparison and decision, orders development, and transition (Headquarters, Marine Corps 2015b). Marine units that are task-organized with planning staffs employ MCPP, usually at the Battalion-level and higher.

- **Problem Framing.** Problem framing is the most important step in MCPP. If leaders misrepresent or misunderstand a problem, even sound planning methodology will result in a solution to the wrong problem. Problem framing identifies what, when, where, and why—resulting in a well-articulated mission statement that conveys commander's intent.
- **COA Development.** Given guidance from the commander on his or her operational approach, this step produces options for accomplishing the mission statement.
- **COA War Game.** This step's purpose is to improve each COA option by inducing friction from opposing planners while manually simulating the scenario. Planners should gain an increased understanding of the situation while evaluating the refined COAs.
- **COA Comparison and Decision.** The commander assesses each COA for its ability to accomplish the mission in accordance with his or her intent. The commander may approve or modify a COA, formulate a hybrid plan, or choose none of them.
- **Orders Development.** This step transforms the commander's decision into information required for execution. The verbal, written, or graphical order guides subordinate planning efforts.
- **Transition.** The final step may include confirmation briefs, rehearsals, or drills that

facilitate execution. The human element is a primary focus of the transition step.

2.2.2 Rapid Response Planning Process

R2P2 mirrors the same six-step process as MCPP, but was developed to allow a Marine expeditionary unit (MEU) to begin action within a compressed 6-hour time frame. The accelerated planning process is enabled by previously developed planning products, timely intelligence, and well-refined standard operating procedures (SOPs). Success is dependent on the concurrent conduct of mission planning and mission preparation (Headquarters, Marine Corps 2015b).

2.2.3 Troop Leading Steps

Troop Leading Steps provides the basic structure for unit leaders to make tactically sound plans in dynamic environments (Headquarters, Marine Corps 2018a). The time-proven process facilitates the detailed analysis of complex information that allows for success in combat. The six steps are: begin planning, arrange for reconnaissance, make reconnaissance, complete the plan, issue the order, and supervise (often abbreviated and referred to as BAMCIS). Step 1 (begin planning) is supported by decision analysis models in Chapter 3 and explored in further detail by Section 2.3.

- **Begin Planning.** This step includes the general tactical thought process. The sub-steps are to conduct an Estimate of the Situation and determine the enemy's most likely course of action (EMLCOA), an exploitation plan, SOM, fire support plan (FSP), and tasks.
- **Arrange for Reconnaissance.** The unit leader gathers questions and assumptions to be confirmed via reconnaissance. Enemy and terrain are primary factors for investigation.
- **Make Reconnaissance.** Leaders validate assumptions and answer questions through physical observation of terrain and the enemy.
- **Complete the Plan.** The SOM is updated as necessary and the Operation Order is written.
- **Issue the Order.** The order is delivered to subordinate units. A confirmation brief may also be delivered to higher-echelon units.

- **Supervise.** Leaders supervise preparation, rehearsals, and execution.

2.3 Tactical Thought Process

This section describes Step 1 of the Troop Leading Steps (BAMCIS), begin planning. Leaders conduct the tactical thought process within Step 1. With an emphasis of tactical thought process as context, we can clearly understand advantages of planning enhancements proposed in Chapter 3.

2.3.1 Estimate of the Situation

The components of an Estimate of the Situation include: Mission Analysis, Enemy Analysis, Troops and Fire Support Available, Terrain and Weather Analysis, and Time Analysis (abbreviated METT-T).

- **Mission Analysis.** The unit leader considers the explicit task and purpose received, enumerating implied actions required to accomplish the assigned mission.
- **Enemy Analysis.** An enemy analysis consists of two parts. The first part requires determining composition, disposition, and strengths of the enemy. This information should include size, activity, location, unit, time, and equipment. The second part requires determining enemy capabilities and limitations in regard to their ability to defend, reinforce, attack, withdraw, or delay.
- **Troops and Fire Support Available.** This step includes the identification of friendly capabilities, limitations, and which units need to detach or attach. Any previously established firing agencies should be identified, along with adjacent or higher unit SOMs.
- **Terrain and Weather Analysis.** Considerations for terrain and weather include observation and fields of fire, cover and concealment, obstacles, key terrain, avenues of approach, and weather (abbreviated OCOKA-W). Observation describes what can be seen from where. Fields of fire are the effects of observation on weapon employment. Observation and fields of fire are imperative—they describe how friendly and enemy units will be able to engage one another. Cover provides protection from enemy fire and concealment provides protection from observation. Obstacles may be natural or man-made and effect the mobility of a force. Key terrain is any area that, when

controlled, provides a significant advantage to either combatant force. Avenues of approach, also referred to as mobility corridors, provide routes for movement and maneuver. Weather is analyzed for temperature and humidity, precipitation, wind, clouds, visibility and those factors' effect on the terrain and forces.

- **Time Analysis.** This step involves identifying the time required to complete each task for mission accomplishment. Time considerations include a breakdown of times between tactical control measures during execution and time allotted for planning, rehearsals, and logistics.

2.3.2 Enemy's Most Likely Course of Action

There are three components to determining EMLCOA: the enemy's mission, current actions, and predicted actions on contact. The enemy analysis conducted in the Estimate of the Situation (METT-T) informs the EMLCOA. A soundly informed and reasoned EMLCOA is a key consideration for leaders while determining a SOM.

2.3.3 Exploitation Plan

In maneuver warfare, leaders analyze the enemy system for a center of gravity and critical vulnerability before devising how to exploit that critical vulnerability. The center of gravity is the factor that allows the enemy to accomplish the mission described in the EMLCOA. When neutralized, the critical vulnerability deteriorates the enemy's center of gravity and hinders mission accomplishment. The exploitation plan communicates a bid to disrupt the enemy system, prohibiting their cohesive mission accomplishment, and enabling friendly mission success.

2.3.4 Scheme of Maneuver, Fire Support Plan, and Task Development

Once the exploitation plan is devised, leaders enact it by generating a SOM that is in accordance with their Estimate of the Situation and EMLCOA. An accompanying FSP is created to outline the use of supporting fires. Tasking statements are generated and the operations order is written and delivered to subordinate leaders. Chapter 3 explains relevant doctrine for creating a supported SOM.

2.4 Air Assault Planning

To understand model applications in Chapter 4, we briefly provide context on the principles of air assault planning. Air assault operations allow for rapid maneuver to achieve a tactical surprise and a massing of forces without hindrance by ground mobility, terrain, or disposition (Headquarters, Marine Corps 2019). The sequence of operations for an air assault is as follows: planning, briefing, loading, air assault, landing, tactical ground operations, sustainment, and ground linkup/air reposition (Headquarters, Marine Corps 2019). Air assault planning requires five basic plans, conducted in reverse order of execution: ground tactical plan, landing plan, air movement plan, loading plan, and the staging plan (Figure 2.3). Due to the reverse planning method, the AFC must produce a timely and comprehensive ground tactical plan to allow the MAGTF to begin their planning and preparation. The AFC must balance the need to produce a plan quickly with the need to produce a plan that will not change upon a more detailed analysis. In this scenario, we improve the planning process for the AFC by providing models to analyze GEOINT in support of mission planning.

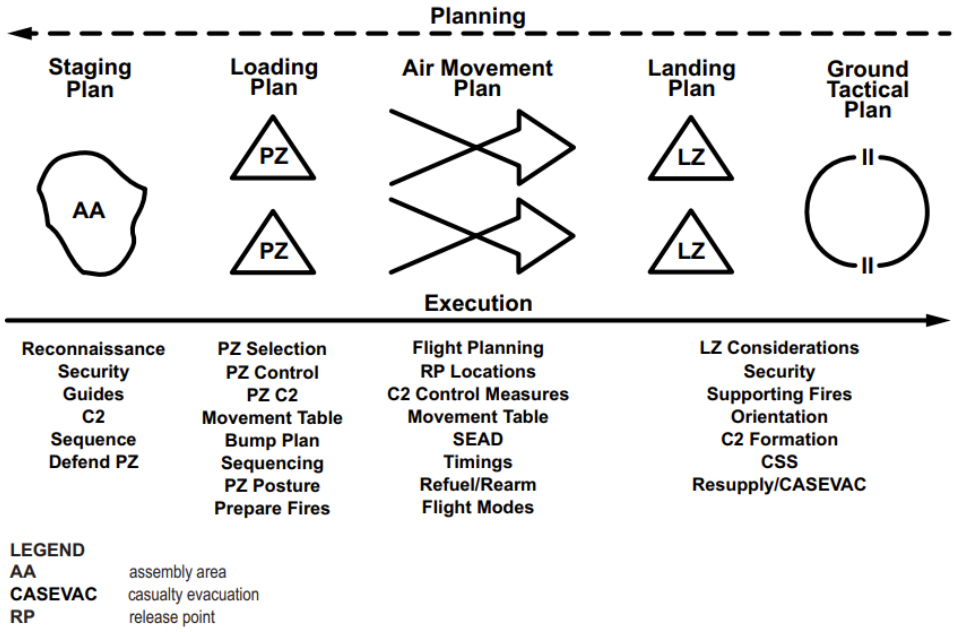

Figure 2.3. Five separate planning phases are required for an air assault, but they must be conducted in reverse order of execution. Required planning tasks are listed under each phase. Source: (Headquarters, Marine Corps 2019).

2.5 Geospatial Intelligence

MCWP 2-10 describes GEOINT as "the exploitation and analysis of imagery and geospatial information to describe, assess, and visually depict physical features and geographically referenced activities on the Earth." The USMC uses geospatial intelligence specialists, residing in topographic platoons, to provide GEOINT analysis products to expeditionary forces. A topographic platoon is only capable of supporting a single Marine expeditionary force (MEF) or up to three MEUs or Special Purpose Marine Air-Ground Task Forces (SPMAGTFs) (Headquarters, Marine Corps 2015a). To support smaller units, a geographic information support team (GIST) of four Marines may be detached to support a battalion of 800 Marines. The centralized and scarce support structure poses a barrier to timely intelligence exploitation and dissemination in distributed operations. To solve this problem, we explore existing models in Section 2.6 that may be applied or extended to support mission planners directly from the platforms described in Section 2.1.1.

2.6 Literature Review

In this section, we examine existing literature for methods relevant to enhancing tactical-level planning. Methodologies from the studies discussed are readily applicable to planning tasks conducted by small-unit leaders. In Chapter 3, we apply and extend these methods to model deliberate attacks in the conduct of an air assault, without the need to rely on geospatial information systems (GIS) software for user interface.

2.6.1 Tactical Pathfinding

There are currently no pathfinding models readily available for small-unit leaders to use during mission planning. Pathfinding methods have been widely researched and implemented, primarily for simulation and video gaming applications. In these cases, agents in virtual environments continuously move to an objective location using paths determined by pathfinding algorithms (Jong et al. 2015). While many pathfinding applications are concerned with the selection of a shortest path, tactical paths balance a compromise between distance and risk. Tactical pathfinding methodology accounts for risk using the assessed risk of terrain and weighted preferences to find the appropriate trade-off between speed and safety.

Pathfinding algorithms return a shortest-path solution across a graph, typically with A* or Dijkstra's search algorithms. In tactical pathfinding, an influence map (IM) or cost-surface raster is generated by weighting terrain risks and adding them to the distance mapping. Weight selection determines the importance of various factors. Factors that determine path speed and risk include surface distance, surface vegetation, slope, elevation, obstacles, and exposure to enemy lines of sight (Kang et al. 2011). The edge cost to reach any adjacent node in the graph is calculated by a weighted sum of these factors (Figure 2.4). This graph is referred to as an IM (Jong et al. 2015) in virtual environments and a cost-surface raster in GIS software (Esri n.d.).

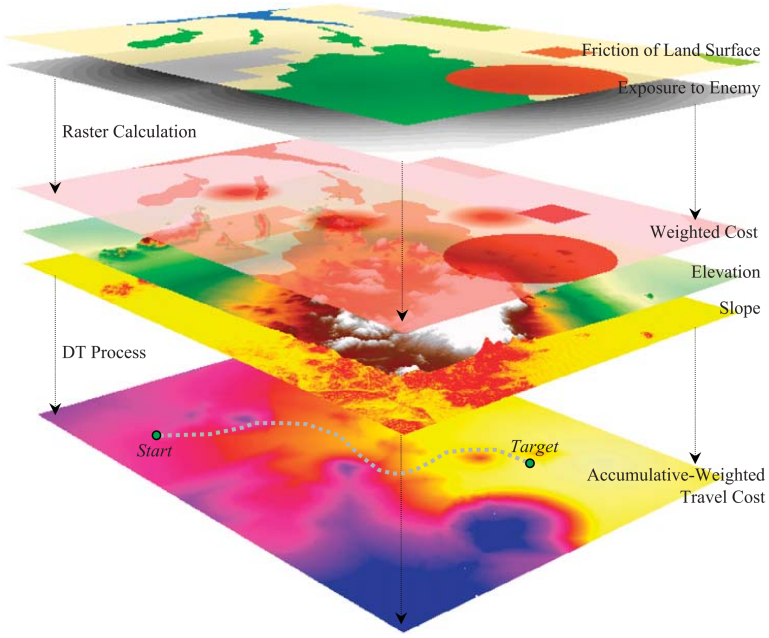

Figure 2.4. Research by Kang et al. (2011) examines GIS-based military pathfinding for an unmanned ground robot (UGR). In this application, a distance transformation (DT) algorithm is used to propagate distances from one cell to another on the cost-surface raster. Various GIS layers are weighted and combined, where the final weighted-travel map (cost-surface raster) is generated and represented as a heat map (labeled *Accumulative-Weighted Travel Cost* in Figure 2.4). The A* search algorithm is then used to find the least-cost path from the start point to the target. Source: Kang et al. (2011).

Selecting risk factor and distance importance weights is critical to achieving the desired trade-off between fast paths and safe paths (Figure 2.5). The sum of risk and distance, multiplied by their importance weights, form the edge costs between neighboring cells in the graph. Shifting importance weights influences the type of path that is chosen.

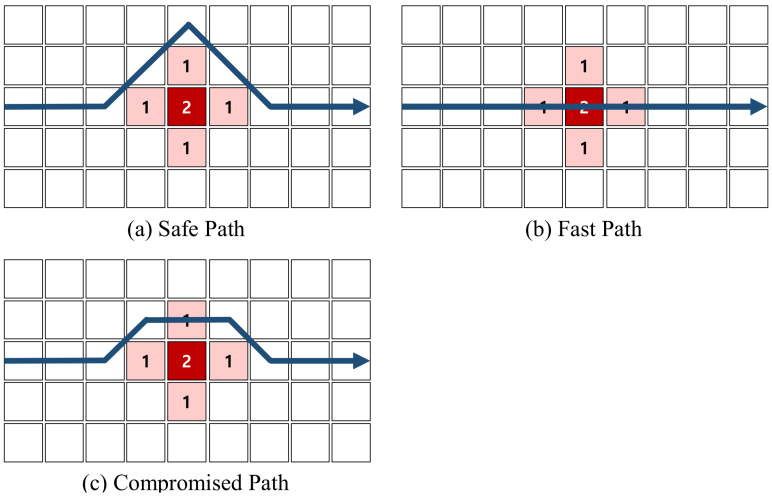

Figure 2.5. Varying importance weights for safety and distance produces different optimal pathfinding outcomes (Jong et al. 2015). Each cell represents travel nodes on the map. Red cells labeled with values represent the quantified risk to travel across those nodes. Path (a) is chosen when the importance for safety is high. Path (b) is chosen when the importance for distance is high. Path (c) represents a compromise between the two competing objectives. Source: Jong et al. (2015).

Jong et al. (2015) conducted experiments to determine how risk and distance measures varied with input weights (Figure 2.6). While safe paths and fast paths can be similar in some scenarios, this is often not the case—safe paths and fast paths have opposite characteristics. Importance weights should be carefully considered because the compromise between distance and safety is often not proportional.

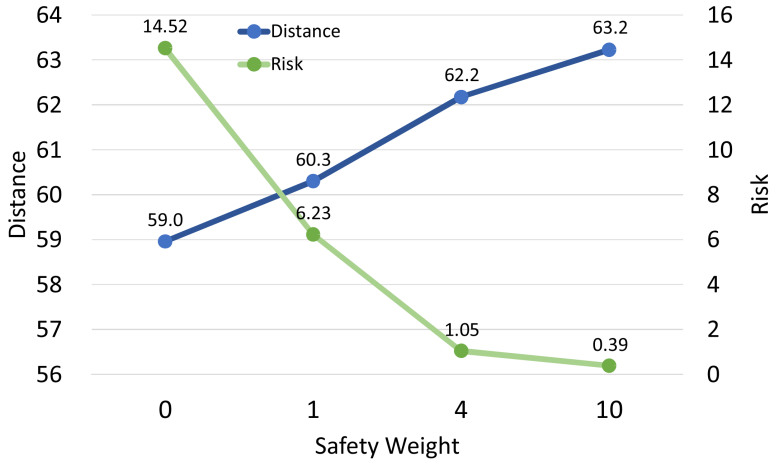

Figure 2.6. Jong et al. (2015) use cumulative distance (blue) and cumulative risk (green) to assess the effects of varying importance weights. In this experiment, the distance weight is held constant at 1 while the safety weight is increased. For two competing objectives, we observe an increase in total distance travelled as overall risk is reduced. In this scenario, the authors also observed variation in the magnitude of risk reduction and distance trade-off as safety importance increased. The data suggests that the benefit of risk reduction outweighs the distance trade-off, especially when safety weight is increased from 0 to 1. Source: Jong et al. (2015).

Research by Kang et al. (2011) provides simulation results for UGR pathfinding tasks in both static and dynamic risk environments. The scenario uses GIS data on elevation and land cover for mountainous regions in Afghanistan, collected from the U.S. Geological Survey (USGS) Seamless database. Figure 2.7 visualizes three least-cost paths for an UGR tasked with moving from Start to Target. The initial path (dashed line) represents the shortest path, accounting for no enemy risk. The second path (pink line) represents risk routing around two known enemy positions (red markers). The third path (green line) represents risk routing around an additional enemy position (yellow marker). Figure 2.7 provides an example, based on real GIS data, for risk-distance trade-off in tactical pathfinding applications.

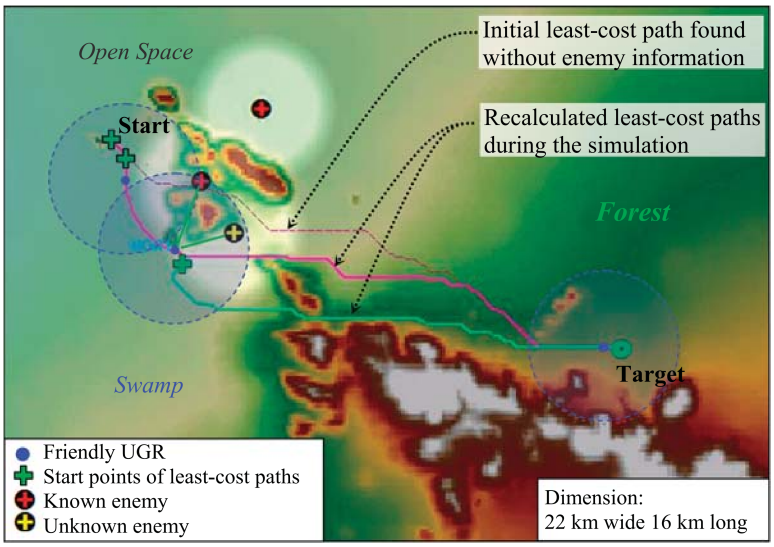

Figure 2.7. After the UGR departs on the initial least-cost path (dashed line), the route is recalculated (pink line) with information for known enemy positions (red markers). Subsequently, the route is again recalculated (green line) when the UGR discovers an additional unknown enemy position (yellow marker). Source: Kang et al. (2011).

2.6.2 Automated Terrain Assessment

Mobility classification and helicopter landing suitability (HLS) overlays are two prominent examples of GIS terrain assessment for military use. While these assessment methods are well developed, their use is restricted to military personnel with training and access to GIS software. Portions of these methods are adapted in Chapter 3 for tactical planning on systems without GIS software, including ATAK for small-unit leaders. We extend the HLS model for a new application in Chapter 3—generating discrete landing boxes.

Passibility classification for cross country movement

Pokonieczny and Wyszynski (2016) present an automated methodology for preparing maps with ArcGIS software to support crisis management. For both crisis management and military operations, decision-makers must be informed on the passibility of cross country terrain when conducting spatial planning. In military applications, these are referred to as movement corridors. North Atlantic Treaty Organization (NATO) provides Standardization

Agreements for the classification of terrain into three categories: GO, SLOW-GO, and NO-GO. Each category has specification thresholds for vegetation, roads, hydrography, urban areas, slope, and elevation variation (Pokonieczny and Wyszynski 2016). As an example, GO terrain requires a slope of less than 30% grade, 30-50% for SLOW-GO, and greater than 50% grade for NO-GO terrain. Pokonieczny and Wyszynski (2016) use GIS software to create classification layers for each criteria, then combine all layers into a collective mobility map. The authors are able to automate the described process, reducing processing time from several days to several hours in the generation of 1:50,000 scale maps.

Pokonieczny (2018) extends his previous work by applying artificial neural networks for terrain classification (Figure 2.8). Instead of discrete classes, the neural network produces a continuous index of passibility (IOP). The neural network was prepared with a training set of 1,000 manually classified grid squares. Using an 80/20% split for training and testing respectively, the Scaled Conjugate Gradient method produced the most accurate activation functions: 82.2% mean testing accuracy for 1000 $\times$ 1000 meter squares, and 95.7% mean testing accuracy for 100 $\times$ 100 meter squares.

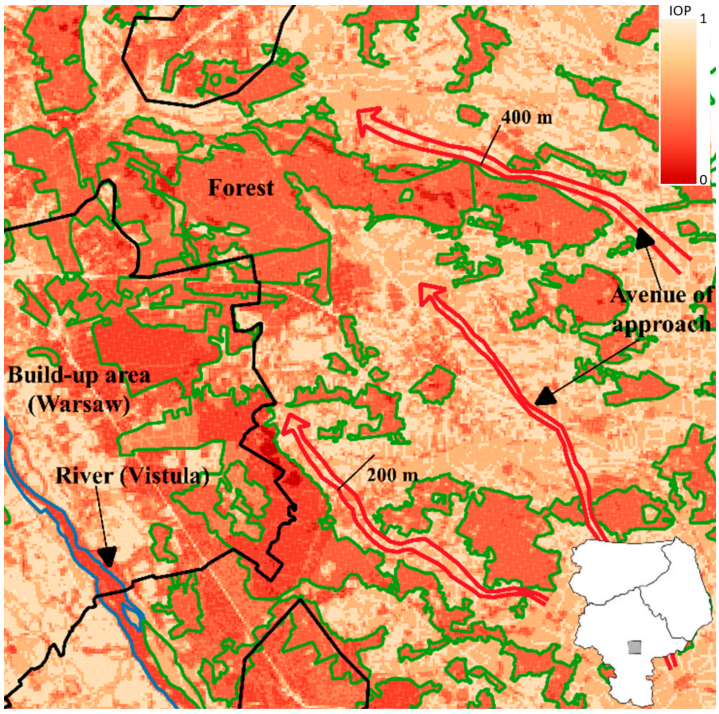

Figure 2.8. A neural net is used to produce a passibility map for 100 × 100 meter grid squares. The heat map coloring indicates the IOP. Avenues of approach are manually drawn in red. Source: Pokonieczny (2018).

HLZ classification

Surveying for suitable HLZ areas and validating tenability is a time consuming process. Kovarik and Rybansky (2014) developed models in ERDAS IMAGINE to filter terrain for HLZ suitability and classify areas large enough for landing formations. HLS overlays can be produced according to requirements defined in the NATO Standardization Agreement for helicopter operations. Apart from avoiding vertical structures and obstacles, there are two additional requirements: ground slope and approach/exit obstruction angle. Kovarik and Rybansky (2014) summarize these conditions as follows:

- Slope should not exceed 7 degrees for daytime operations, or 3 degrees for nighttime operations.
- Obstruction angle to obstacles should not exceed 6 degrees for 500 meters for daytime operations, and 4 degrees for 3000 meters for nighttime operations.

Once the HLS overlay has been created, suitable areas may be algorithmically tested for the desired number of landing points. The output of this method is a binary terrain overlay suitable for further investigation. Naturally, as the number of desired landing points increases, the area of suitable HLZ terrain decreases.

While Kovarik and Rybansky (2014) and others have provided research on automated HLZ selection methods, little study has been done to quantify the accuracy of these methods. Erskine et al. (2022) address this by examining the effect of data resolution on the accuracy of detected HLZs (Figure 2.9). For 12 known HLZs in three varying geographic regions, the authors of the study quantify accuracy of proposed HLZs produced from data of spatial resolutions varying from 1 meter to 30 meters (Figure 2.10). Accuracy was assessed by measuring the mean distance from vertices on the boundary of the identified HLZ from the reference boundary. Erskine et al. (2022) concluded that HLZ accuracy increased with resolution, although the level of acceptable resolution varied greatly depending on the geographic characteristics of the test region.

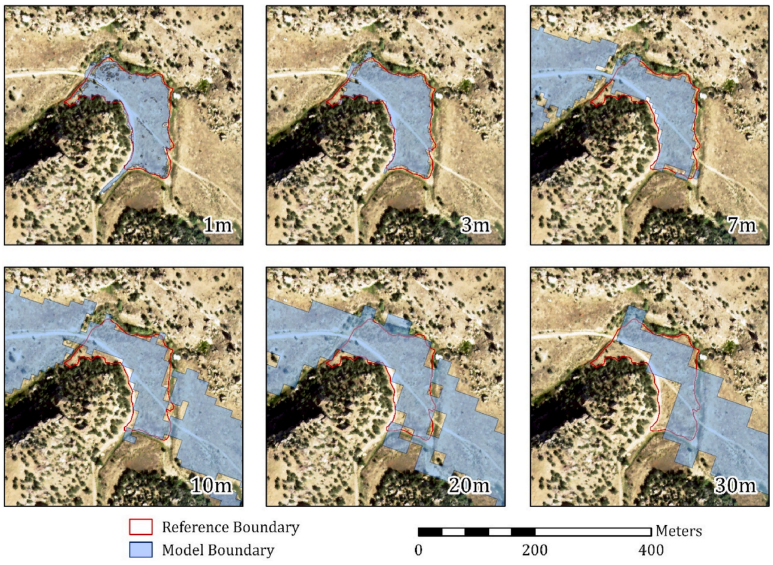

Figure 2.9. Varying data resolution produces different HLZ boundaries for Site 7. Shaded regions represent boundaries produced by the model, while the red outline presents the reference boundary. Source: Erskine et al. (2022).

Figure 2.10. For each resolution on the x-axis, 12 sites were evaluated for mean error—deviation from the reference boundary, measured in meters. Error increases as resolution decreases, with variation induced by the geography of the specific site. Source: Erskine et al. (2022).

CHAPTER 3:
Methodology

In Chapter 3, we begin by describing the geospatial data selected for our models, summarizing how each observation is represented, and the assumptions and limitations associated with the data. In Section 3.3, we review the process for creating a HLS overlay and describe the model for generating discrete landing boxes from that information. Section 3.4 describes the application of viewsheds; this is context for viewshed use as data layer inputs in subsequent sections. Section 3.5 provides the minimum-cost or minimum-risk flow formulation and a sample scenario for the tactical pathfinding model. Section 3.6 describes planning considerations for the employment of machine guns in support of an offensive maneuver and the model for enumerating employment position choices. We conclude in Section 3.7 with a model formulation for selecting an optimal COA for an air assault. A broad workflow diagram for these models is given in Figure 3.1.

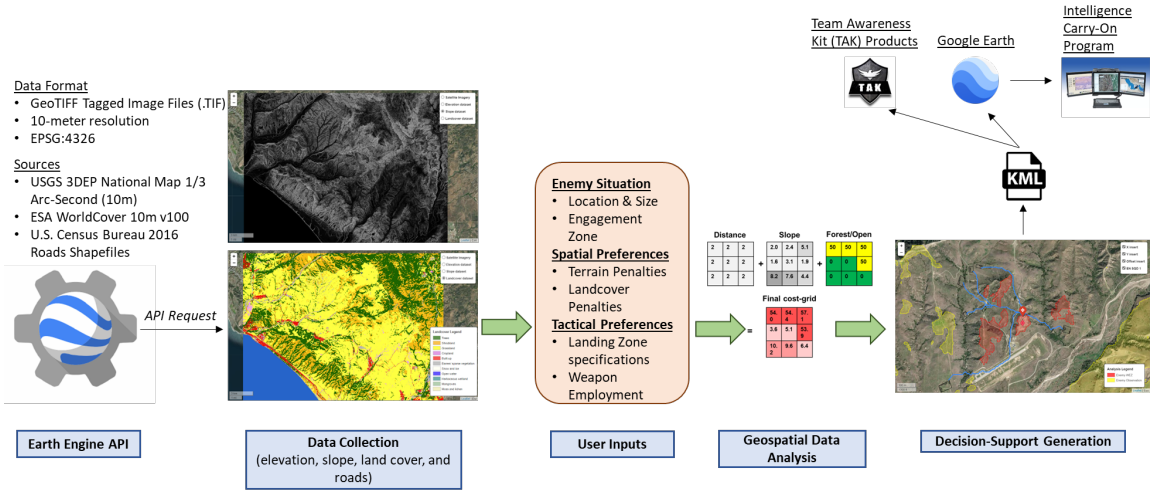

Figure 3.1. An overview workflow diagram describing methodology implementation. Geospatial data are analyzed in accordance with user inputs and preferences. The resulting analysis graphics and metadata are written to Keyhole Markup Language (KML) for interoperability with Google Earth and TAK products.

3.1 Geospatial Data

We use three types of datasets to support our analysis: elevation, land cover, and roads. These datasets are collected and maintained by various organizations including the USGS, the European Space Agency (ESA), and the U.S. Census Bureau. Each organization hosts data as different file types, such as GeoTIFF and Shapefile. However, all three sources are seamlessly available through the Earth Engine Data Catalog (Google Earth Engine n.d.). The Google Earth Engine application programming interface (API) is used to clip selected regions of interest, calculate slope, and write GeoTIFF files with a single desired resolution and geographic coordinate system for all three datasets. The resulting GeoTIFF files represent a raster (gridded-area) of the region of interest, with data values assigned to all coordinates within each grid square. For the purposes of this analysis, the selected resolution for each grid square is approximately 10 meters by 10 meters.

3.1.1 Digital Elevation Model

A digital elevation model (DEM) is a "digital cartographic gridded representation of the elevation of the Earth's surface at regularly spaced intervals in x and y directions, using z-values referenced to a common vertical datum" (National Geospatial-Intelligence Agency 2019). For this thesis, we selected the 1/3 Arc-second (approximately 10 meter) DEM from the USGS National Map 3D Elevation Program (3DEP). The elevation values in this DEM are represented in meters and correlate to topographic bare-earth surface (U.S. Geological Survey 2020). This DEM's coverage is limited to the contiguous U.S., Hawaii, Puerto Rico, territorial islands, and parts of Alaska (U.S. Geological Survey 2020).

3.1.2 Land Cover

Land cover or land use datasets classify the ground surface composition of the Earth. We selected the ESA WorldCover 10m v100 dataset (Zanaga et al. 2021), a 10-meter resolution global land cover product. The ESA WorldCover 10m v100 product is based on both Sentinel-1 and Sentinel-2 data from 2020, yielding 11 land cover classes (Table 3.1) that were independently validated with a global average accuracy of 75% (ESA WorldCover n.d.). A subsequent version of the product was released on October 28th, 2022 with an increased global accuracy of 76.7% (ESA WorldCover n.d.).

Table 3.1. A description of data contained within the ESA WorldCover 10m v100 land cover dataset. There is one categorical variable with 11 levels for land cover type, listed by coding in the Classification Code column. The adjacent column lists the ground composition classification description. Source: Google Earth Engine (n.d.).

Classification Code	Classification Description
10	Tree cover
20	Shrubland
30	Grassland
40	Cropland
50	Built-up
60	Bare / sparse vegetation
70	Snow and ice
80	Permanent water bodies
90	Herbaceous wetland
95	Mangroves
100	Moss and lichen

3.1.3 Roads Shapefiles

Shapefiles "spatially describe vector data such as points, lines, and polygons, representing, for instance, landmarks, roads, and lakes" (U.S. Census Bureau 2016). We utilized the Topologically Integrated Geographic Encoding and Referencing (TIGER) U.S. Census Roads shapefiles dataset (US Census Bureau 2016), which was prepared by the U.S. Census Bureau in the 2016 release. The all-roads shapefile includes over 19 million line features for primary roads, secondary roads, local neighborhood roads, rural roads, city streets, vehicular trails, ramps, service drives, walkways, alleys, and private roads, reflecting changes made to the database through May 2016 (U.S. Census Bureau 2016).

3.1.4 Google Earth Engine API

The USGS 3DEP 1/3 Arc-second DEM, ESA WorldCover 10m dataset, and TIGER: U.S. Census Roads dataset are all available through the Earth Engine Data Catalog. Google Earth Engine is a geospatial processing service powered by the Google Cloud Platform (Google Developers n.d.), with available APIs for Python and Javascript. We utilized the *Export.image* client library to build a Python script for loading the datasets, clipping data to a desired region, calculating slope from the DEM, masking the roads Shapefile to a binary raster, and writing and downloading the three files in GeoTIFF format (Table 3.2). The slope array is stored as the second band in the DEM GeoTIFF. All datasets are downloaded with uniform location, shape, resolution, and coordinate reference system (CRS).

Table 3.2. The Earth Engine *Export.image* client formats and downloads data from the API. Client arguments are listed in the first column, with an argument description in the adjacent column. The input column describes client inputs used for retrieving our data. Source: Google Developers (n.d.).

Argument	Description	Input
image	Image to export.	Image raster for each dataset
filename	Name for file download.	*'prefix_datatype.tif'*
scale	Resolution in meters per pixel.	*10*
region	Clip shape to export.	Rectangle object
crs	CRS to export in.	*'EPSG:4326'*

3.1.5 Raster Representation

The *rasterio* Python library is used to read gridded GeoTIFF files downloaded from Earth Engine. In total, three rasters are read into the program, with the DEM containing two bands for elevation and slope. Each raster grid cell may be referenced by its row and column index or any coordinate that lies within the grid cell. All raster parameters are summarized in Table 3.3 and visualized in Figure 3.2.

Table 3.3. A 10-meter by 10-meter gridded representation of the AO is produced once the data are downloaded and read. Any grid cell in our raster may be referenced by row and column or longitude and latitude. All coordinates within a cell are assigned four parameters: elevation, slope, land cover, and road use.

Raster cell parameters	Data type	Unit
reference	integer or float tuple	*(row, col)* or *(longitude, latitude)*
elevation	float	meters
slope	float	degrees
land cover	integer	land cover classification
road	booloean	*1* for road, *0* for non-road

(a) Bare satellite imagery

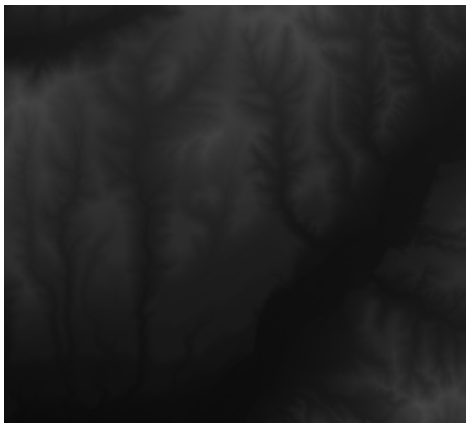

(b) Elevation: darker regions are lower

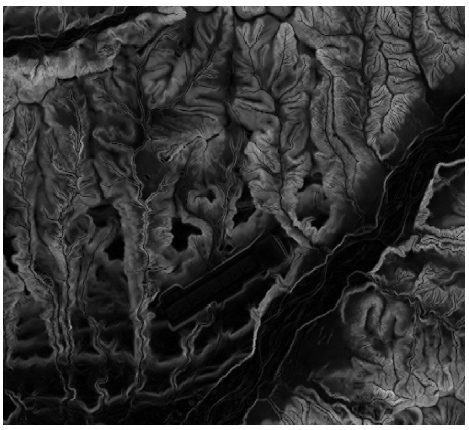

(c) Slope: darker regions are flatter

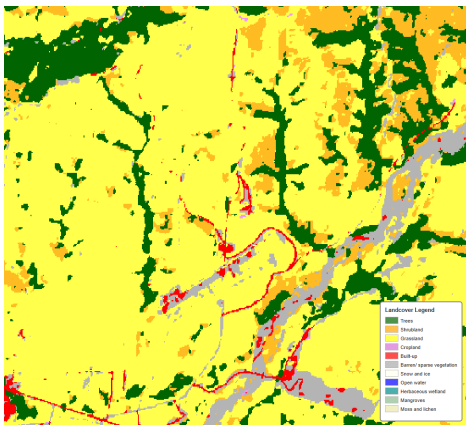

(d) Land cover: classifications by color

(e) Roads: black cells represent road classifications

Figure 3.2. Geospatial raster data may be visually represented with plots and map overlays. (HOLF, Camp Pendleton, California)

3.2 Assumptions and Limitations

The open-source nature of our geospatial data provides some limitations to our methodologies. Limitations include the absence of data sets for vertical obstructions, infrastructure, and a digital surface model (DSM). Regardless of whether the data is open-source or a National Geospatial-Intelligence Agency (NGA) product, there are inherent limitations with respect to resolution, accuracy, and timeliness. Assumptions relate to the simplification of land cover data when calculating viewsheds.

3.2.1 Assumptions

- **Vegetation density.** Data pertaining to vegetation density are not used, therefore sweeping assumptions are made about visibility in forested areas. For instance, when calculating viewsheds, the user decides whether to treat forest terrain as absolutely concealed or absolutely unconcealed. This decision should be made based on seasonality, imagery intelligence, and the end-user's exercise of military judgement.
- **Movement speed.** The user must assume a base movement pace for traversing terrain. We segment paces between forest and non-forest movement speed to allow for more refined control of the movement time estimate. A correction for elevation gain is applied, based on Naismith's rule which allows for an additional hour for every 600 meters of ascent (Magyari-Sáska and Dombay 2012).

3.2.2 Limitations

- **Timeliness.** The land cover and elevation data used were published in 2020. Changes to the vegetation or geography of regions that occur over time may reflect as errors in our results. Road data only reflects changes made to the census database through May 2016 (U.S. Census Bureau 2016).
- **Slope and Aspect.** The Earth Engine client library *Terrain.slope* calculates slope from the 4-connected neighbors of each cell, averaging all four slope values (Google Developers n.d.). This may not provide an accurate representation of the passibility of micro-terrain, depending on the resolution of the DEM. Additionally, aspect calculations were not exported from Earth Engine. For pathfinding, the effort to travel between two cells may be reduced if the two cells share the same aspect angle, and the direction of travel is perpendicular to that angle.

- **Resolution and precision.** For most open-source elevation products, 10 meters is the highest resolution available. It is possible that greater precision may be gained from NGA products, whose use may improve results at the cost of computational efficiency and memory.
- **Accuracy.** As of 2022, USGS 3DEP 1/3 arc-second products were compared to 25,000 known survey points for a root mean square error (RMSE) of 0.82 meters (U.S. Geological Survey 2020), improved from 1.55 meters in 2013.
- **Data availability.** On the Earth Engine Data Catalog, road data and 10-meter DEM resolutions are only available for the U.S., with few exceptions. DEM products at this resolution for foreign countries are not available at the unclassified level.
- **Vertical obstructions and infrastructure.** Our datasets do not encompass information pertaining to vertical obstructions, such as overhead power lines, or other infrastructure-related obstacles and features.
- **Digital Surface Model.** A DSM "depicts the elevation of the top of buildings, trees, towers, and other features elevated above the bare earth" (National Geospatial-Intelligence Agency 2019). We do not have the ability to quantify the effects of forest canopy height or urban structures during viewshed analysis without a DSM.

3.3 Generating Helicopter Landing Zones

> The primary goal of military HLZ identification is to locate useable areas prior to an operation, often under time and resource constraints, so models must be efficient and able to work with minimal data.
>
> —Erskine et al. (2022)

HLZs are critical for determining points of insert or extract during helicopter-borne military operations. HLZ identification is conducted during the mission planning process and requires input from subject matter experts (SMEs), execution force leaders, and intelligence products prepared on GIS software. When using GIS software, the first step in HLZ production is to generate a HLS overlay (Erskine et al. 2022). After the HLS overlay has been produced with the methods described in Section 3.3.1, we explore using machine learning techniques to parse suitable terrain for more user-ready HLZ identification (Section 3.3.2).

3.3.1 Helicopter Landing Suitability Overlays

Rasterized slope and land cover data are routinely used by military and civilian organizations to create HLS overlays (Kovarik and Rybansky 2014). When using raster data to filter terrain for suitability, the overlay will refer to a per-pixel area that meets specified criteria (Kovarik and Rybansky 2014). For our model, we define a suitable overlay as containing pixels meeting the following two requirements:

- **Slope.** Suitable overlay area should contain terrain with slope less than or equal to a user-defined threshold. Generally, 7 degrees is considered acceptable, with up to 15 degrees considered possible (Erskine et al. 2022). Thresholds may be more conservative for nighttime operations and vary by Type/Model/Series of aircraft. Individual specifications are available per Type/Model/Series per aircraft orientation with regard to the upward slope.
- **Land cover.** Grassland and barren terrain are the two land cover classes we consider as suitable for our model's HLS overlay.

Once the suitability parameters are defined, we generate the HLS overlay with basic array masking operations. The process begins by filtering the land cover dataset for pixels that are barren or grassland. With an array of acceptable land cover, we subtract terrain that is steeper than our defined slope threshold. The process is described by a workflow diagram in Figure 3.3, plots of the binary arrays in Figure 3.4, and a satellite overlay of the final HLS in Figure 3.5.

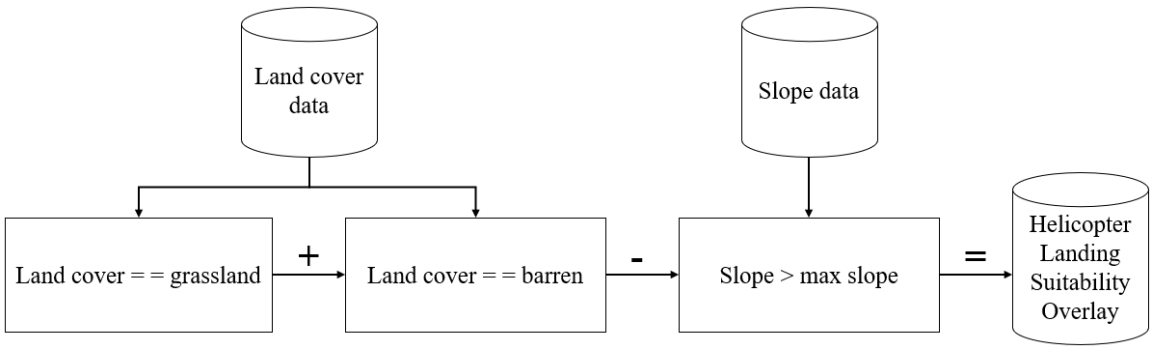

Figure 3.3. A workflow diagram for generating HLS overlays from land cover and slope raster data.

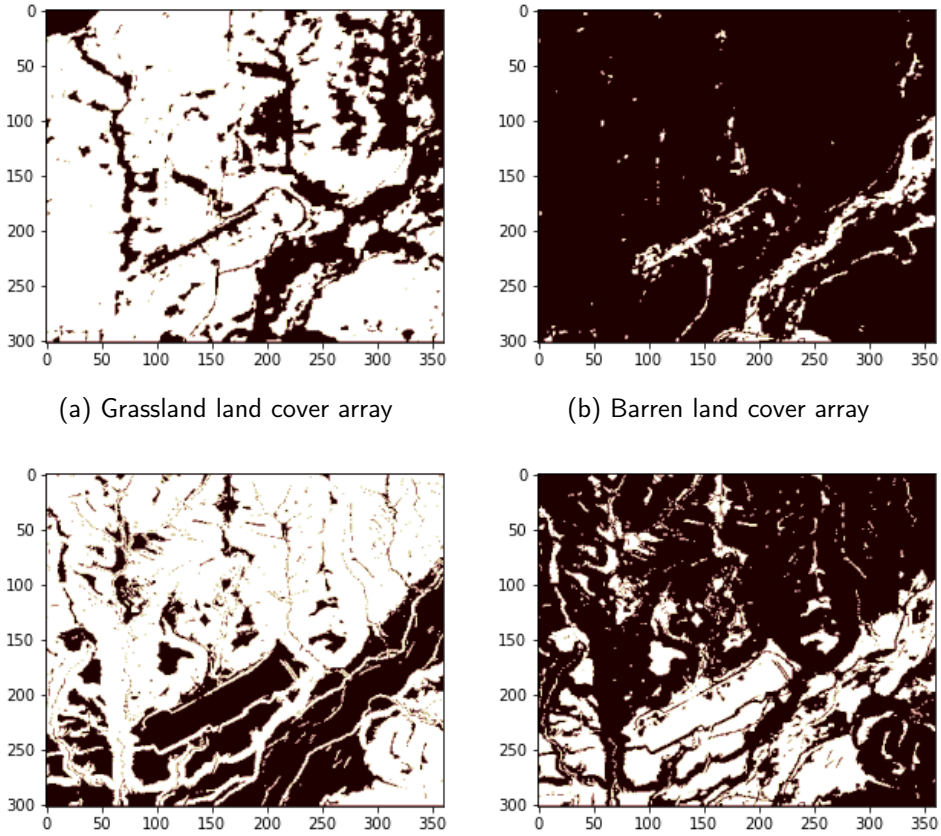

(a) Grassland land cover array

(b) Barren land cover array

(c) Slope array for values exceeding threshold

(d) Combined HLS array

Figure 3.4. A visual representation of the workflow diagram presented in Figure 3.3. Pixel values are *1* (white) if sub-caption criteria is met and *0* (black) if sub-caption criteria is not met. To generate the combined HLS overlay, we add together the masks for grassland and barren land cover, then subtract the mask for sloped pixels that are greater than the slope threshold. This model was run for the HOLF, Camp Pendleton, California, with a slope threshold value of 7 degrees. Figure 3.2 (d) may be referenced to compare how land cover data was filtered.

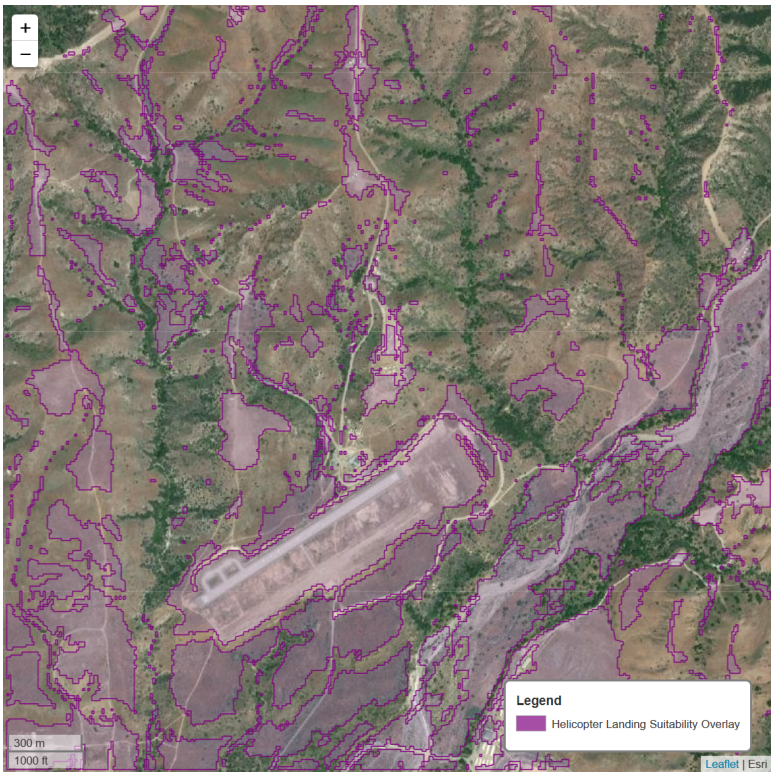

Figure 3.5. A satellite overlay of the HLS array generated in Figure 3.4. The shaded region represents pixels that are grassland or barren and less than 7 degrees slope.

Recall from Chapter 2.6.2, Erskine et al. (2022) provided research on the relationship between data resolution and accuracy for HLS overlays generated with this method. The authors recognize that HLZ accuracy is typically qualitatively assessed as there are no accuracy standards established by the NGA. In order to quantify uncertainty for commanders and planners who rely on these products, Erskine et al. (2022) conducted accuracy assessments (Figure 3.6) for 12 sites in three geographic regions, at 10 resolutions ranging from 1 meter to 30 meters. Note that the study did not use the same data sources as this thesis, so the accuracy assessment is not directly applicable to our models. However, the results provide useful insights as to the accuracy of this method and factors that affect reliability.

The three geographic locations studied included West Point, Fort Carson, and Joint Base Elmendorf-Richardson. These regions respectively provided terrain samples for a forested environment with many mountains, ridges, and valleys; a flat and arid environment with

valleys and mesas; and a forested environment with rolling hills. Accuracy was assessed by measuring the distances of vertices from selected HLZ polygons to a reference boundary. The average error distance from the reference boundary was reported as the mean error for that resolution at that site (Erskine et al. 2022).

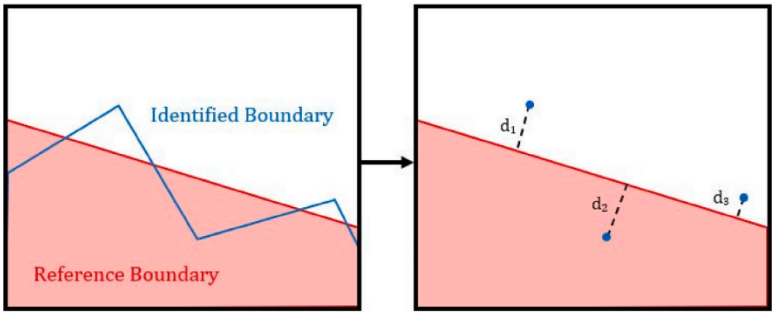

Figure 3.6. Erskine et al. (2022) assess HLZ accuracy by measuring the distances between identified HLZ vertices and reference boundary vertices, denoted as d_n. The average of all d_n values for a HLZ is reported as the mean error. Source: Erskine et al. (2022).

Upon inspection of the 10-meter resolution results from Table 3.4 and Table 3.5, we find that this method performs strongly at sites bounded by forests and pronounced terrain (West Point and Joint Base Elmendorf-Richardson) with Average Mean Errors of 5.77 and 10.08 meters respectively. However, at 10-meter data resolution this method struggled in the flat arid environment of Fort Carson with an Average Mean Error of 45.19 meters. Practical lessons from the study may be summarized as follows:

- Generally, there is a positive correlation between data resolution and HLZ accuracy across all sites.
- The lowest resolutions acceptable were observed to be between 5 and 10 meters.
- Regions with well-defined boundaries, whether by sloping terrain or vegetation, produced more accurate HLZs.
- Sites that produced the highest levels of error contained disrupting features within the HLZ. At lower resolutions these obstacles were not represented in the data.

Table 3.4. Erskine et al. (2022) conducted an accuracy assessment across three locations and 12 sites, producing a table of mean error statistics by input data resolution. Source: Erskine et al. (2022).

Data Resolution (m)	1	5	10
Minimum Mean Error (m)	1.51	2.39	3.43
Maximum Mean Error (m)	21.03	21.89	90.72
Mean Error Range (m)	19.53	19.50	87.29
Average Mean Error (m)	6.30	5.84	19.99

Table 3.5. Erskine et al. (2022) conducted an accuracy assessment across three locations and 12 sites, producing a table of mean error statistics by input data resolution and geographic region. Source: Erskine et al. (2022).

Data Resolution (m)	1	5	10
WEST POINT (5 Sites)			
Minimum Mean Error (m)	1.51	3.04	4.16
Maximum Mean Error (m)	3.49	4.36	9.55
Mean Error Range (m)	1.98	1.32	5.39
Average Mean Error (m)	2.61	3.56	5.77
Median Mean Error (m)	2.83	3.50	5.12
FORT CARSON (4 Sites)			
Minimum Mean Error (m)	2.04	2.39	3.43
Maximum Mean Error (m)	21.03	21.89	90.72
Mean Error Range (m)	18.99	19.50	87.29
Average Mean Error (m)	12.76	9.53	45.19
Median Mean Error (m)	13.98	6.92	43.30
JBER (3 Sites)			
Minimum Mean Error (m)	3.42	3.80	5.13
Maximum Mean Error (m)	4.25	5.89	18.85
Mean Error Range (m)	0.83	2.09	13.71
Average Mean Error (m)	3.85	4.70	10.08
Median Mean Error (m)	3.87	4.42	6.25

3.3.2 Helicopter Landing Zone Selection

While the HLS overlay is helpful for initial planning of Air Assault Operations, it has not yet been fully processed into information that is readily consumable by decision makers. During the planning phase of Air Assault Operations, HLZs are selected by the AFC and assault flight leader (AFL), the ground officer in command of the air assault force and the aviator in command of the assault support flight (Headquarters, Marine Corps 2019). Marine Corps

Tactical Publication (MCTP) 3-01B, *Air Assault Operations* (Headquarters, Marine Corps 2019) provides recommended HLZ dimensions and considerations for different types of aircraft, shown in Table 3.6. MCTP 3-01B also provides the following guidance for HLZ selection, applying both to landing zone (LZ) and pickup zone (PZ) sites:

- The ground must be suitable for the safe landing of aircraft—firm enough to prevent bogging down. If the ground is determined to be unsuitable, a hover during loading or unloading may be necessary.
- The site should be identifiable from the air.
- The site is covered from interference by enemy fires.
- The ground must be as level as possible. Slopes greater than 7 degrees require examination by the AFL and air mission commander (AMC).
- The site must be free of obstacles and loose debris such as heavy dust, light snow, logs, rocks, or dry grass. Obstacles that cannot be removed should be marked and identified to the aircrew.
- The ingress route should allow for landing in a direction that is into the wind, with tailwinds of no more than 5 knots.

Table 3.6. A table of recommended HLZ specifications adapted from MCTP 3-01B, *Air Assault Operations* (Headquarters, Marine Corps 2019). Detailed information may be found in current aircraft Navy tactics, techniques, and procedures (NTTP) publications.

	HLZ Dimensions (m)		
Type	Single Aircraft	Section (2 Aircraft)	Other Considerations
CH-53	60×90	90×120	Large rotor wash
MV-22	50×55	95×100	Large rotor wash
UH-1Y	20×20	45×45	Variety of missions and ordnance
AH-1	20×20	45×45	Narrow skids require flat, smooth surface
UH-60	30×30	60×60	Medical evacuation (unarmed)

Generating landing boxes from HLS regions

Since human decision-makers require rectangular HLZ dimensions to assess landing box specification adherence, we aim to further distill the HLS overlay into suitable landing boxes. The *shapely* Python library provides a useful and efficient method to do this for each of our HLS polygon objects, called *minimum_rotated_rectangle()*. Once a bounding rectangle is drawn, we scale down and relocate the rectangle until it is sufficiently contained within the HLS region.

To begin, we define s_{factor} as the scale factor for each iteration, ϵ as the non-HLS area tolerance, and d_{min} as the minimum acceptable length and width. For every suitable polygon in the HLS overlay, we draw its *minimum_rotated_rectangle()* to create our working landing box (LZ_Box in Algorithm 1). This begins a continuous loop that occurs while the non-suitable area error is greater than our ϵ threshold. On each iteration, we scale down the box by factor s_{factor}, relocate the landing box to the polygon's centroid, and check to see that both dimensions are still greater than d_{min}. If the scale and relocation didn't achieve the desired tolerance, we also crop the HLS polygon by our newly scaled landing box and re-draw the shape without the excluded areas. HLZ candidates that meet tolerance and size requirements are recorded as HLZs. We describe this process in Algorithm 1 and Figure 3.7.

Algorithm 1 HLS Polygon to HLZ landing box algorithm.

```
s_factor ← 0.9
ϵ ← HLZ error tolerance
d_min ← minimum HLZ length and width
landing_zones ← list()

for polygon in HLS_overlay do
    LZ_Box ← polygon.minimum_rotated_rectangle()
    within_tolerance ← False
    while percent unsuitable terrain within LZ_Box > ϵ do
        scale LZ_Box down by s_factor
        relocate LZ_Box to polygon centroid
        if LZ_Box dimensions <= d_min then
            break
        end if
        if percent unsuitable terrain within LZ_Box > ϵ then
            remove polygon areas outside of LZ_Box
            re-draw LZ_Box with new clipped polygon
        end if
    else
        within_tolerance = True
    end while
    if within_tolerance == True then
        append LZ_Box to landing_zones list
    end if
end for
```

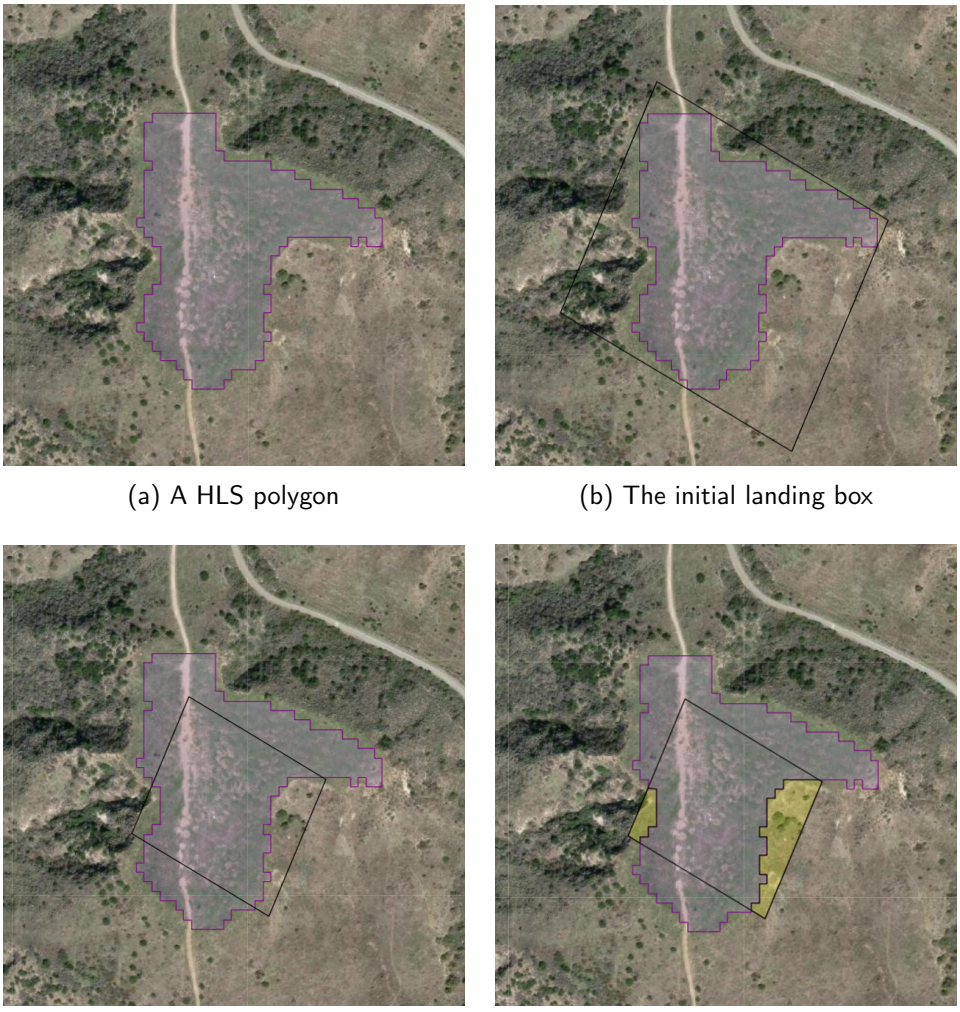

(a) A HLS polygon

(b) The initial landing box

(c) Down-scaled landing box

(d) Highlighted error within landing box

Figure 3.7. A visualization of the HLZ generation process using the *shapely* Python library. Recall that the original HLS polygon from (a) represents area that is suitable for an HLZ. We generate a landing box from this shape in (b) by applying the *minimum_rotated_rectangle()* method to the HLS polygon. Figure (c) shows the updated landing box after several iterations of down-scaling. In Figure (d), we highlight (in yellow) the unsuitable terrain contained within the landing box. We set the stopping limit for the algorithm by defining a maximum error threshold, known as ϵ in Algorithm 1, that limits the maximum percent error contained within the landing box.

Sub-division of complex HLS regions

Consequently, this algorithm struggles to effectively use the complex and particularly non-convex shapes within our HLS overlay. To increase performance, we sub-divide complex shapes into more manageable parts for the landing box generating algorithm. This is achieved by transferring the latitudes and longitudes of all representative cells to a data frame and applying an unsupervised machine learning method to classify clusters of geospatial coordinates. This produces a dataset where all adjacent observations are separated by equal distances. Due to the homogeneous density across observations, we investigated k-means, spectral, and hierarchical clustering as methods of classification.

Each of the selected clustering methods require the manual specification of number of clusters, $n_{clusters}$. We determine this number algorithmically by Equation 3.1, where ϵ_{HLZ} is the initial error percentage of the bounding landing box, and n_{max} is the maximum number of clusters. In our test cases, we use $n_{max} = 7$ and a condition where the program will decide to cluster before drawing landing boxes when the initial ϵ_{HLZ} is > 0.40.

$$n_{clusters} = \max\{2, round(\epsilon_{HLZ} n_{max})\} \tag{3.1}$$

Continuing with the same HLS polygon used in Figure 3.7, we show the clustering results of each of our selected methods in Figure 3.8. A dendrogram for hierarchical clustering is given in Figure 3.9. Each of the labeled sub-shape data frames are translated back into polygons, and re-run through the landing box generation process described by Algorithm 1 and Figure 3.7. By applying clustering to complex HLS regions, we increase the total HLS utilization and reduce the unsuitable landing area within generated landing boxes.

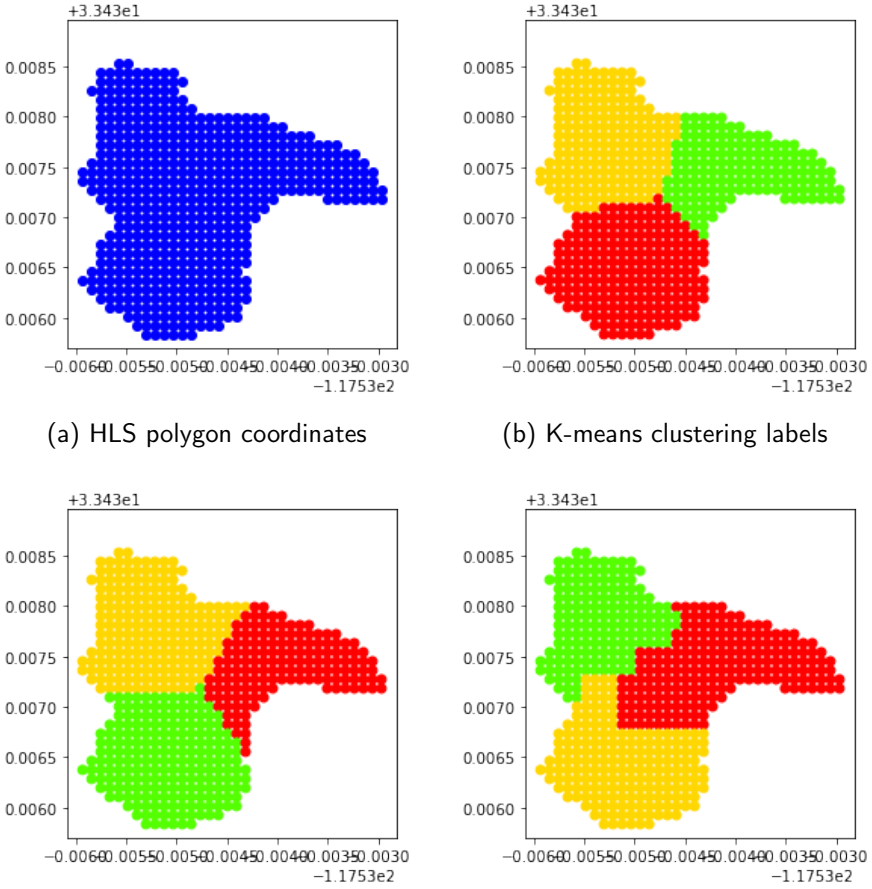

(a) HLS polygon coordinates

(b) K-means clustering labels

(c) Spectral clustering labels

(d) Hierarchical clustering labels

Figure 3.8. A visualization of the HLS polygon clustering process. The error of the initial bounding box is assessed to be greater than 0.40, so this polygon is selected for clustering. Equation 3.1 determines that $n_{clusters} = 3$. We see a plot of the data frame of representative points in (a), followed by the classification labels for each clustering method in (b) through (d). The x and y axes represent the longitude and latitude for each representative raster cell.

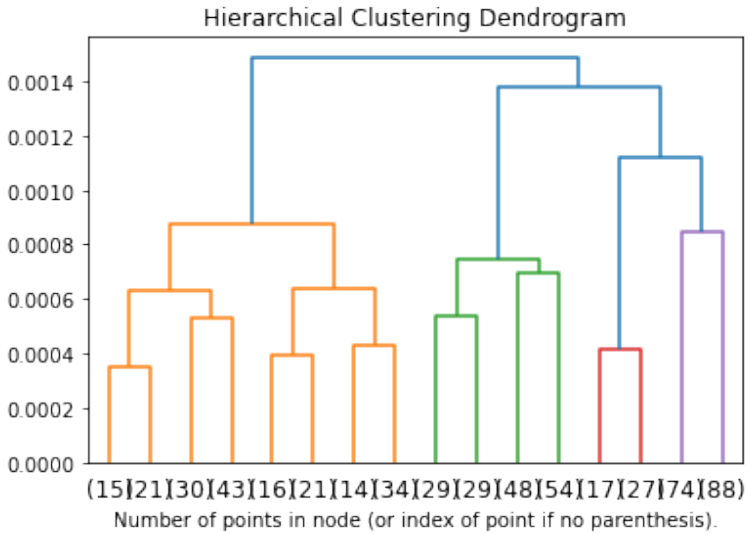

Figure 3.9. A classification dendrogram for the clusters produced by hierarchical clustering in Figure 3.8 (d). Colors correlate to the assignment of labels used in the same Figure. In this application, we selected the average linkage metric as criteria for the merge strategy.

Assessing HLZ generation effectiveness

To discern between the effectiveness of each of the three clustering methods, we propose the percentage of the overall HLS area utilized by our HLZ boxes as a measure of effectiveness. Percentage of HLS utilized, as described by Equation 3.2, is calculated by taking the area of the intersection of all identified HLZs and the HLS overlay, divided by the total area of the HLS overlay.

$$HLS_{utilization} = \frac{Area_{HLZ \cap HLS}}{Area_{HLS}} \tag{3.2}$$

where, $Area_{HLS}$ = the area of the total HLS region

$Area_{HLZ \cap HLS}$ = the total area of the HLS region utilized by generated HLZs

Using percent HLS utilization as our measure of effectiveness, we run four versions of the HLZ generation model: with no clustering, k-means, spectral, and hierarchical clustering.

The four models were run for the same region we generated our HLS overlay (Figure 3.5)—the HOLF, Camp Pendleton, California. This region is characterized by intervening draws, fingers, ravines, and hills that produce complex polygons in our HLS overlay. We run the experiment across 10 slope threshold levels, from 3 to 13 degrees. Polygon complexity increases with the slope threshold, generally decreasing model performance. The experiment was also run with two levels of percent error tolerances for individual HLZs, $\epsilon = 0.10$ and $\epsilon = 0.15$. The results for both iterations are shown in Figure 3.10.

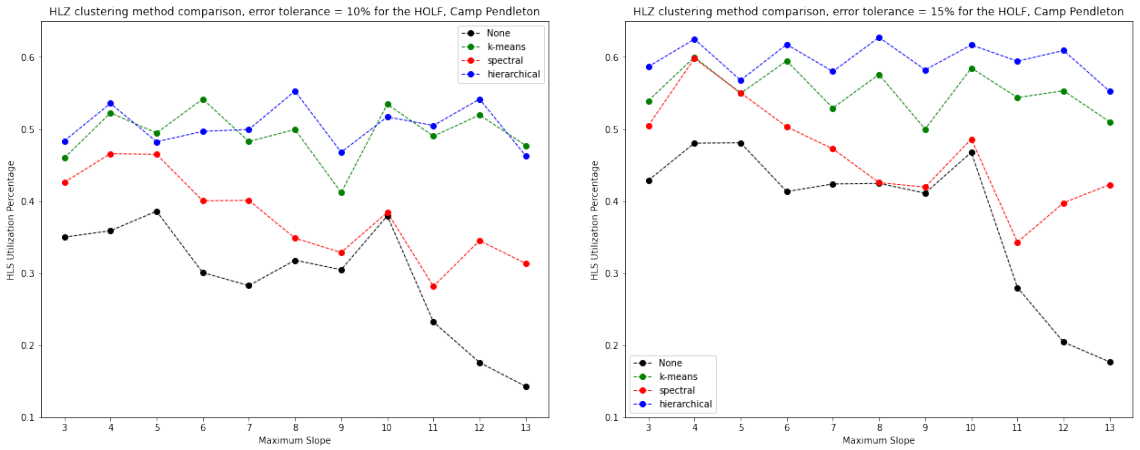

(a) Error tolerance = 0.10

(b) Error tolerance = 0.15

Figure 3.10. An experiment was run across two error tolerance levels and 10 slope threshold levels for the HLZ generation model at the HOLF, Camp Pendleton, California. Each set of parameters were given as inputs to four methods for dividing complex HLS shapes: no clustering, k-means clustering, spectral clustering, and hierarchical clustering. The response of interest is percent utilization of the HLS, as described by Equation 3.2.

We observe that k-means and hierarchical clustering perform nearly uniformly with varied error tolerance and HLS polygon complexity. In contrast, the performance with spectral clustering and without clustering falls precipitously as slope threshold and HLS polygon complexity increase. Performance between k-means and hierarchical clustering appears to be comparable, so we investigate the results of similarly performing data points for qualitative differences. Figure 3.11 shows the satellite overlay for an error tolerance of 15% and slope threshold of 7 degrees. Since the utilization percentages for k-means and hierarchical

clustering are relatively comparable at these input levels, we are able to observe qualitative differences without bias on overall performance. We find that hierarchical clustering has a greater tendency to generate overlapping HLZs, perhaps contributing to its increased performance at higher error tolerance thresholds. In contrast, k-means appeared to produce more tightly packed, non-overlapping HLZs. Since the measure of distance used by k-means is Euclidean in this application, the clusters produced are more likely to be geometrically contiguous.

(a) K-means clustering, 52.9% utilization

(b) Hierarchical clustering, 58.0% utilization

Figure 3.11. An overlay of the results of two data points from the experiment in Figure 3.10. The error tolerance was set to 15% and slope threshold at 7 degrees.

3.4 Viewshed Analysis for Friendly and Enemy Positions

For military planning applications, a predominant benefit of DEMs is the ability to conduct a viewshed analysis. Without a viewshed analysis, lines of sight must be estimated from a map study or confirmed during a leader's reconnaissance prior to execution of the mission. Not all mission sets, such as air assault operations, facilitate conditions for on-the-ground reconnaissance prior to execution. All models presented in this chapter incorporate information derived from a viewshed analysis, allowing decision-makers to analyze friendly and

enemy interactions with the terrain before setting foot on the ground.

For viewsheds, we utilize the Python libraries *xarray* and *xrspatial*. These libraries provide functions that return a binary visibility raster from input parameters and elevation data. Input parameters include observer location, observer height, and target height. In our appli-cation, we add two additional parameters—maximum weapon engagement zone (WEZ) and maximum observation range. Maximum WEZ is used to delineate portions of the viewshed that are within a unit's field of fire and portions for which the unit can only observe the terrain. Maximum observation range is used to clip the DEM to a smaller region, increasing computational efficiency. Viewshed shapes and weights are available for use as parameters in other models, notably in the tactical pathfinding model.

We do not make use of a DSM in addition to the DEM, so calculations are only made from data on the height of bare earth surface. For vegetation and urban terrain, we allow the decision-maker to choose whether to treat those landcover classes as concealed or unconcealed. We provide an example viewshed overlay for two enemy positions in Figure 3.12.

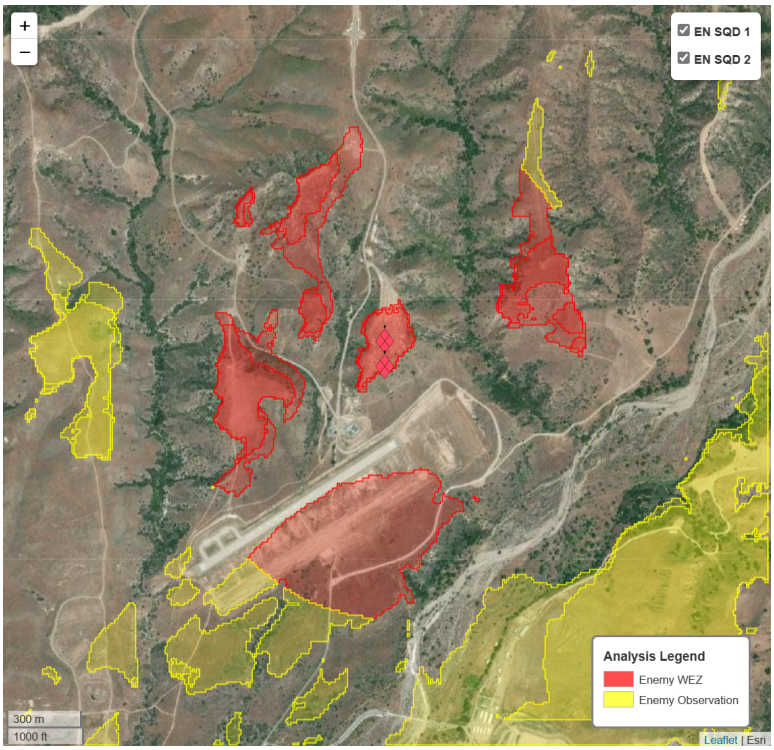

Figure 3.12. A viewshed analysis overlay for two enemy positions. Red regions represent terrain within line of sight and within their maximum WEZ, while yellow regions represent terrain that is observable, but outside maximum WEZ. The northern enemy position has a height of 4 meters, the approximate height of a building in the urban center. The southern enemy position has a height of 2 meters, the assumed upper bound on the height of a standing human. Both positions have a maximum WEZ of 1,000 meters, observable distance of 1,500 meters, and target height of 2 meters.

3.5 Tactical Pathfinding

During the mission planning process, the ground force commander must consider the strengths, weaknesses, and risks associated with decisions involving friendly and enemy use of terrain. We provide models to understand those factors for HLZs in Section 3.3, lines of sight from friendly or enemy positions in Section 3.4, and machine gun employment geometries in Section 3.6. As key terrain features are considered as a source of influence for friendly or enemy forces, unit leaders must also consider their influence on routes or paths traversed in the execution of the mission.

Recall from Chapter 2.6.1, tactical pathfinding is used in geospatial analysis to find the shortest path while accounting for risk. The fundamental trade-off for tactical paths is the compromise of speed and security, otherwise described as distance and risk. We account for risk by weighting each layer of our data and model results, then summing the penalized layers together to create a single cost-grid raster for our AO. The weights for each layer are determined by the decision-maker's use case and represent their relative risk assessment for the terrain. We solve for the shortest or minimum-cost path between two points on the cost-grid raster with Dijkstra's or A* algorithms. A lower penalty weight correlates to a lower relative risk assessment for that layer. The layers requiring weighting and a sample weight profile are described in Table 3.7.

Table 3.7. A summary of data layer weights when building the cost-grid raster to solve for minimum-cost path. The weighted values of each data layer are summed together, forming a cost-grid raster that represents the decision-maker's risk assessment for the AO. Since we are solving for minimum cost path, higher weights correlate to higher risk.

Layer	Data type	Example weight profile
Landcover risk assessment		
Open terrain	boolean	50
Shrubland penalty	boolean	25
Forested terrain	boolean	0
Urban terrain	boolean	50
Road use	boolean	75
Water	boolean	nC (numeric infinity)
Slope risk assessment		
Terrain slope	float (degrees)	5
Enemy risk assessment		
Observable to enemy	boolean	75
Enemy field of fire	boolean	100
Distance risk assessment		
Base grid cost	1	50

As applied in this case, tactical pathfinding may be described as a minimum-cost flow network problem. Each grid in the cost-grid raster serves as a network node and the node adjacency list is enumerated using the 8-Neighbors method—the four cells bounding the origin node and its four diagonals. The decision variable, X, is a binary choice of whether to traverse to one cell from another. In the objective function (Equation 3.3), flow costs are the destination cell cost from the cost-grid raster. Equation 3.4 describes the flow balance constraints for cell path selection. Equation 3.5 ensures binary cell path selection for the decision variable.

Index use [~ cardinality]

$i \in N = \{1, 2, ..., n \text{ nodes}\}$	node index [~ n]
$k \in K = \{\textit{open, shrubland, forest, urban, road, slope, etc.}\}$	data layer [~ 10]
A set of 8-Neighbor adjacency node pairs	node adjacency list [~ $n \cdot 8$]

Given Data

$raster_{i,k}$	geospatial raster observation for node i in layer k
$penalty_k$	penalty weight for layer k

Decision Variables

$$X_{i,j} = \begin{cases} 1 & \text{if path between node } i \text{ and } j \text{ selected} \\ 0 & \text{otherwise} \end{cases}$$

Formulation

$$\min_X \quad \sum_{(i,j)\in A} X_{i,j} \sum_{k=1}^{10} raster_{j,k} penalty_k \tag{3.3}$$

$$\text{s.t.} \quad \sum_{j:(i,j)\in A} X_{i,j} - \sum_{j:(j,i)\in A} X_{j,i} = \begin{cases} 1 & \text{if } i = s \\ -1 & \text{if } i = t \\ 0 & \text{otherwise} \end{cases} \quad \forall i \in N \tag{3.4}$$

$$X_{i,j} \in \{0, 1\} \quad \forall (i, j) \in A \tag{3.5}$$

One tactical scenario may call for a fast and risk-assuming path, while another scenario require the most risk-adverse path of any distance. In our proposed model, the sensitivity control for this compromise is the *base grid cost* parameter. A low or zero *base grid cost* will cause the algorithm to not penalize the traversal of extra grid cells, resulting in a longer, more risk adverse path. A higher *base grid cost* will dilute the relative risks of other data layers, resulting in a shorter, more direct, and more risk-assuming path. Since the objective function value is a unitless measure of risk, we output summary measures of effectiveness (MOE) for each risk objective.

We perform an experiment for a pathfinding scenario at the HOLF, Camp Pendleton. The cost-grid rasters and minimum cost paths for three levels of *base grid cost* are shown in Figure 3.13. A satellite overlay of the resulting paths are shown in Figure 3.14, and MOEs are given in Table 3.8.

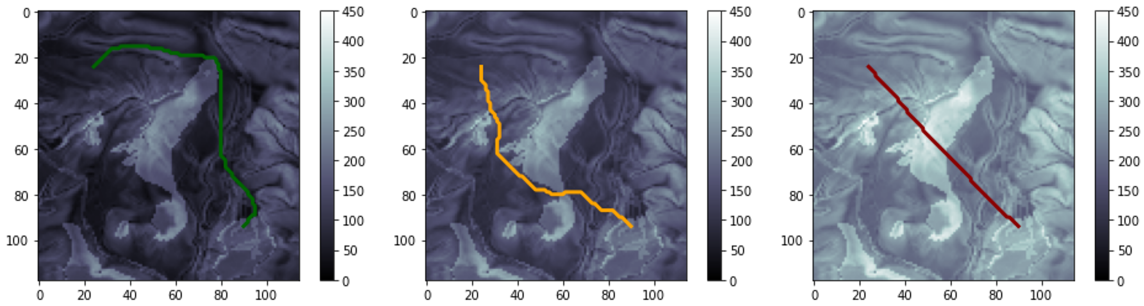

Figure 3.13. Cost-grid rasters and differing minimum cost paths when *base grid cost* is varied between 0 (green), 50 (orange), and 150 (red). All other penalty weights are held constant at the levels described in Figure 3.14.

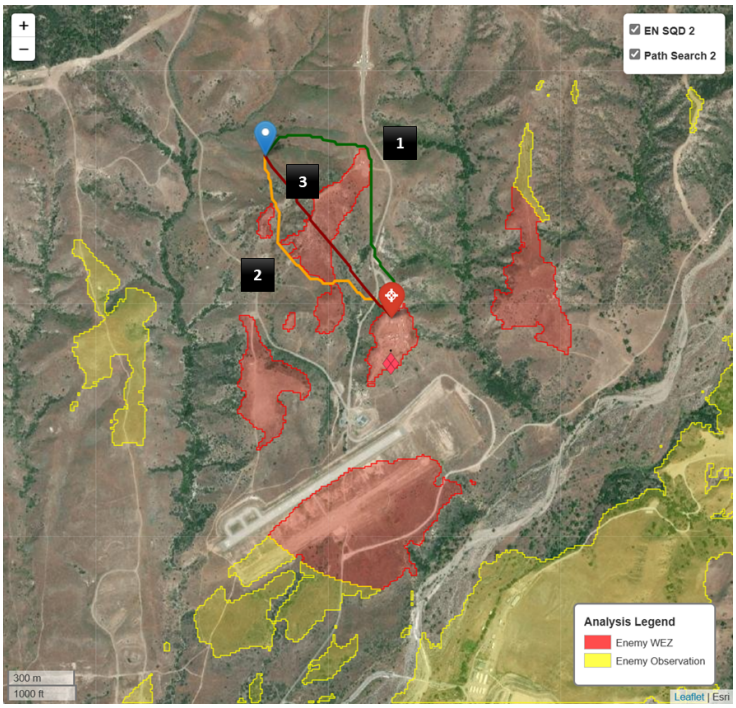

Figure 3.14. A risk sensitivity analysis for tactical pathfinding at the HOLF, Camp Pendleton. Red areas represent terrain that is within the enemy field of fire and yellow represents observable terrain beyond their engagement distance. Each colored path represents a shortest path with varying degrees of risk sensitivity. In all three scenarios, input risk weights were held constant at levels described in Table 3.7, with the exception of Open and Shrubland penalties that were set to zero. Path 1 (green) has a distance weight of 0, Path 2 (orange) has a distance weight of 50, and Path 3 (red) has a distance weight of 150. The summary MOEs for this multi-objective shortest path are summarized in Table 3.8.

Table 3.8. A table of summary MOEs for the risk sensitivity experiment described by Figure 3.14. As the tolerance for risk increases with distance weight, we observe that the overall path length decreases. However, elevation gain increases along with exposure to the enemy WEZ. Travel time calculated using Naismith's rule shows that time travelled may not decrease with overall distance due to the length of time added by traversing steep terrain.

Path	1	2	3
Distance Weight	0	50	150
Total distance (m)	1320.3	1056.8	903.3
Travel time (minutes)	25.3	22.2	22.1
Elevation gain (m/ft)	84.8/278	94.7/311	112.6/369
Elevation loss (m/ft)	-65.8/-216	-75.7/-248	-93.6/-307
Concealed (m)	20.5	0	0
Unconcealed (m)	1299.8	1056.8	903.3
Enemy field of fire (m)	20.5	53.9	175.6
Observable (only) to enemy (m)	0	0	0
Road use (m)	51.2	21.6	25.1

3.6 Support by Fire Generation

> In the offense the preferred method for employing the M240G is by section from a base(s) of fire from which the guns can mass their fires in a continuous, accurate, heavy volume that will produce a telling effect against enemy personnel and equipment. The weight of massed medium machine gun fire is significant and must not be underestimated.
>
> —MCTP 3-01C, Headquarters, Marine Corps (2021)

During offensive operations, commanders and small-unit leaders must plan to provide maneuvering units with cover by fire when cover or concealment by terrain is no longer

available. For providing suppression (cover by fire) from a support by fire (SBF) position, medium machine guns are the most effective weapon system organic to a rifle company table of organization and equipment (T/O). In the attack, the assault position is the last covered and concealed position located between the line of departure and the objective (Headquarters, Marine Corps 2018a). To preserve economy of fires and minimize risk to both the supporting and maneuver forces, it is imperative for commanders to select a combination of maneuver route and SBF position that minimizes distance between the assault position and the objective.

Battlespace geometries constrain employment locations for SBF positions. For machine guns, prohibitive geometries include the surface danger zone (SDZ) (Figure 3.16) the minimum safe line (MSL) of the gun-target line (GTL). A ground-to-ground SDZ encompasses that portion of the earth and the air above in which personnel or equipment may be endangered by ground weapons firing or demolition activities (Department of the Army 2014). For maneuver, DA-PAM 385-63 specifies a MSL from the GTL of 15 degrees or 100 meters, whichever is more restrictive (Department of the Army 2014). With the approval of range deviations or by discretion in combat, commanders may maneuver with the less restrictive MSL rule and deviate closer than 100 meters to the GTL. For the maneuvering force, distance between shifting or ceasing of suppression is minimized by approaching the objective at a 90 degree angle relative to the GTL (Figure 3.15).

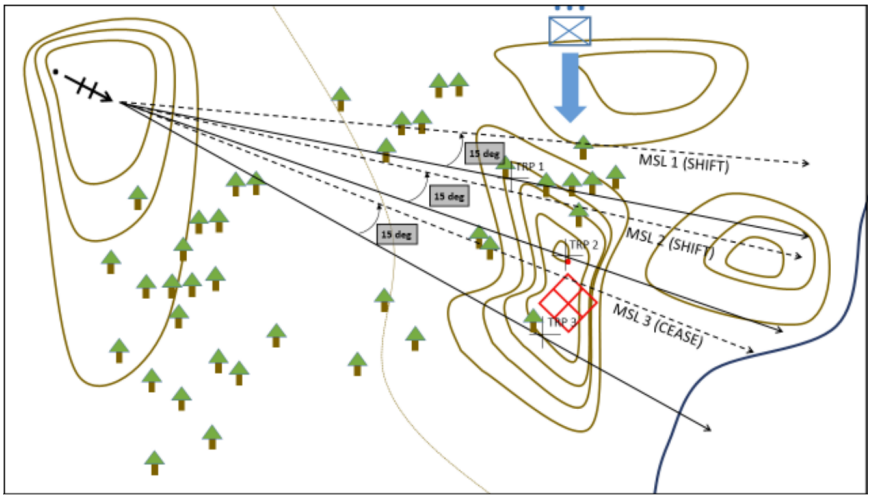

Figure 3.15. An example of offensive medium machine gun employment in support of a maneuvering unit. Solid arrows represent GTLs to each target reference point (TRP) and dashed arrows represent the MSL for each GTL. Fire shifts to the subsequent TRP as each MSL is tripped, ceasing at MSL 3. To receive support for the maximum distance possible, the maneuvering force (blue) approaches with a 90 degree flanking offset to the GTL. Source: The Basic School, Marine Corps Training Command (n.d.).

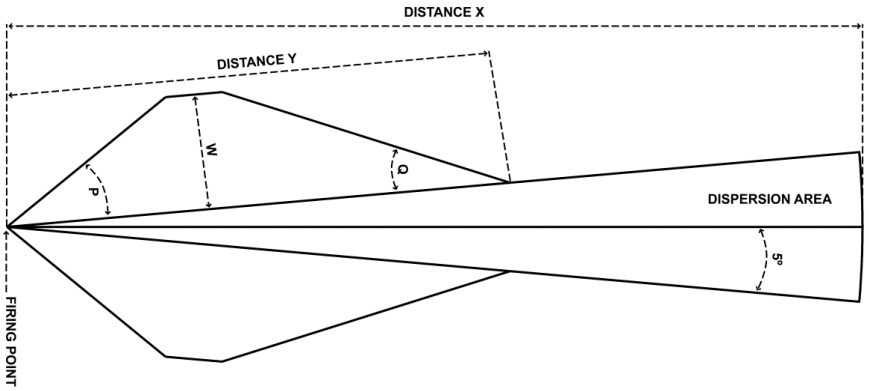

Figure 3.16. The batwing SDZ for firing small arms direct-fire weapons without exploding projectiles. The M240G firing M80 7.62mm Ball ammunition has a Distance X of 4,100 m, Distance Y of 4,073 m, Distance W of 1,461, Angle P of 43.54 degrees, Angle Q of 38.90 degrees, and ricochet vertical hazard of 706 m. The probability of a projectile escaping SDZ boundaries is 1 in 1,000,000. Source: Department of the Army (2014).

To generate possible SBF positions, we run a viewshed analysis from each TRP. The default observer height is one meter, center mass of a standing human and the ideal cone of fire center for the trajectory of a grazing machine gun burst. The default target height is zero meters, for tripod-mounted machine gun employment from the ground. The range is set to the max effective range of a M240G, 1,800 meters. The resulting SBF suitability overlay is the intersection of all viewsheds calculated from each TRP (Figure 3.17). For decision-support use and to generate data layers for COA generation, we plot the GTL, MSL, and SDZ for any SBF position selected (Figure 3.18).

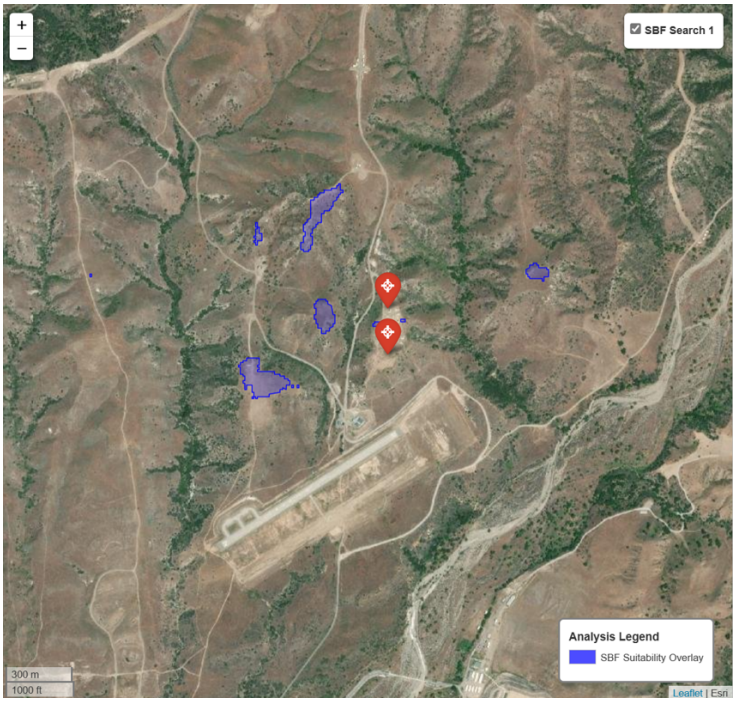

Figure 3.17. A SBF suitability overlay generated for a friendly tripod-mounted M240G tasked with suppressing the two TRPs represented by red markers. Blue regions represent the feasible location options for a commander to employ a medium machine gun section.

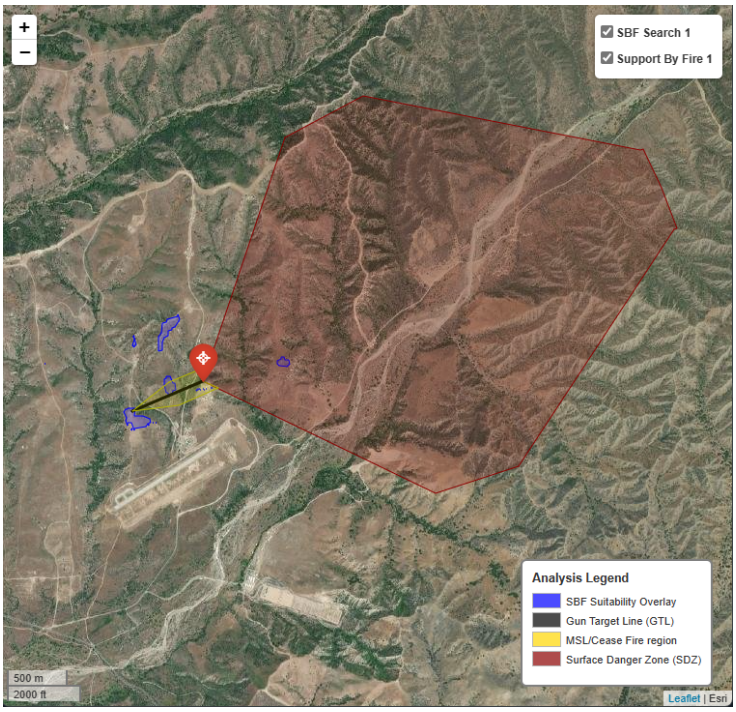

Figure 3.18. An overlay of the GTL, MSL, and SDZ for a selected SBF position. The GTL (black) describes the firing trajectory between the firing point and the target. When friendly troops are maneuvering to the target, the MSL (gold) describes the region in which firing along the GTL must cease for safety. For safety beyond the GTL, the SDZ (red) is the region in which a projectile has less than a 1 in 1,000,000 probability of escaping.

3.7 Course of Action Optimization

We have provided models for determining three critical COA decisions during planning for an offensive air assault: a HLZ generation model, tactical pathfinding generation model, and SBF generation model. In our sample scenario, we have generated 192 possible HLZs, 682 possible SBF locations, 2 choices of TRPs to gain a foothold, and discretized 3 maneuver path options for each selection combination. This results in a total feasible solution space of 785,664 COAs.

When the choice of HLZ, SBF, and TRP are viewed as "stages," we are provided the framework to formulate this problem as an acyclic network (Figure 3.19 (a)). Each of the three critical decisions represent a "stage" of nodes, where each node is a choice

generated by our models. Connectivity between subsequent nodes has inherent dynamic complications. The choice of SBF position will result in a different arc cost based on decisions from the preceding HLZ stage and the subsequent TRP stage. Furthermore, the tactical pathfinding model serves as the objective function and optimizer—it is solved in one iteration with a combination of stage decisions as inputs. For these reasons, this problem is most appropriately formulated as a branch-and-bound problem with a single root node and numerous dummy nodes created to enumerate each combination of stage nodes (Figure 3.19 (b)). As this method results in an extreme number of branch plans, we may induce sparsity into the model by filtering for HLZ qualities such as aircraft type and spreading out the minimum distance between possible SBF positions. After enumerating the multi-objective function values for all branch plans, we can return the best COAs for several key MOEs to the user. This may include returning the plan that minimizes total time for execution, time exposed to enemy fields of fire, or distance travelled without concealment.

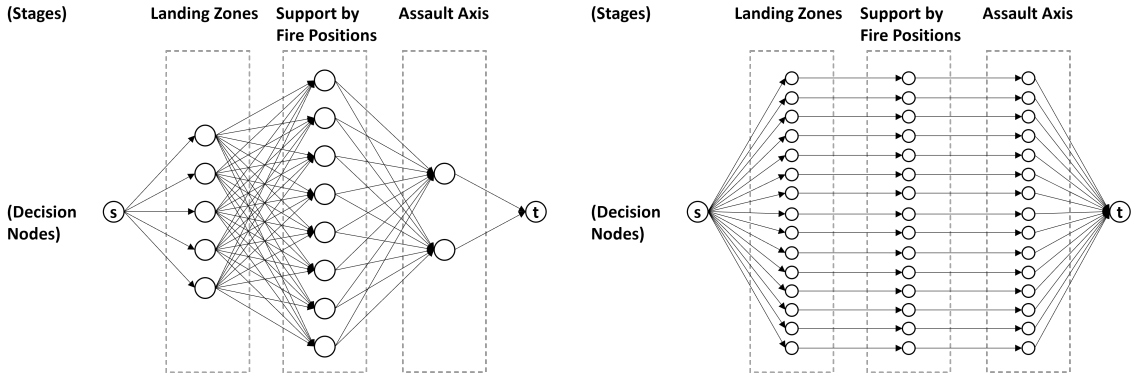

(a) Initial network formulation

(b) Branch-and-bound formulation

Figure 3.19. Network graphs representing COA optimization formulation. Figure (a) represents an initial acyclic network formulation of the problem, which is divided into three stages: choice of HLZ, choice of SBF, and choice of assault axis (by selection of TRP). This formulation presents two infeasible complications. First, the problem has a dynamic nature—the cost of one decision is impacted by the preceding and successive decisions chosen. Second, the tactical pathfinding model is used as the optimizer. This model requires all stage-wise decision inputs to solve for shortest path in one iteration. Figure (b) shows a more accurate problem formulation, where dummy nodes are created and all combinations of stage decisions are generated as a branch-and-bound problem with a single root node.

THIS PAGE INTENTIONALLY LEFT BLANK

CHAPTER 4:
Results

In Chapter 4, we describe the results of constraining the COA optimization scenario described in Section 3.7. Once the problem is properly constrained, we discuss the objective function evaluation method and the multi-objective optimization used to return optimal solutions meeting the commander's evaluation criteria. Finally, we discuss the optimization results and computational efficiencies of each model proposed.

4.1 Course of Action Constraints

In Chapter 3.7, we described an enumerated 785,664 COA branch plans. These plans are generated by a combination of the 192 HLZs, 682 SBF positions, 3 pathfinding risk tolerance levels, and 2 choices of location to make entry to the objective. We add several constraints to the model to pre-screen undesirable solutions and reduce the total feasible solution space.

First, we reduce the total number of possible HLZs by requiring that the LZ dimensions be large enough to accommodate at least a section (two aircraft) of MV-22 simultaneously. We further reduce the number of HLZs by removing any that are not covered from enemy observation or direct-fire weapons. The removal of uncovered HLZs is accomplished by updating the viewsheds for enemy units in the AO for observation of a target of height 6.73 meters, the height of an MV-22. These viewsheds are combined and any HLZs not disjoint from this region are removed. This reduces the number of possible HLZs from 192 to 12. Of the remaining 12 HLZs, 6 are in close proximity to another—they are manually removed from the subset (Figure 4.1).

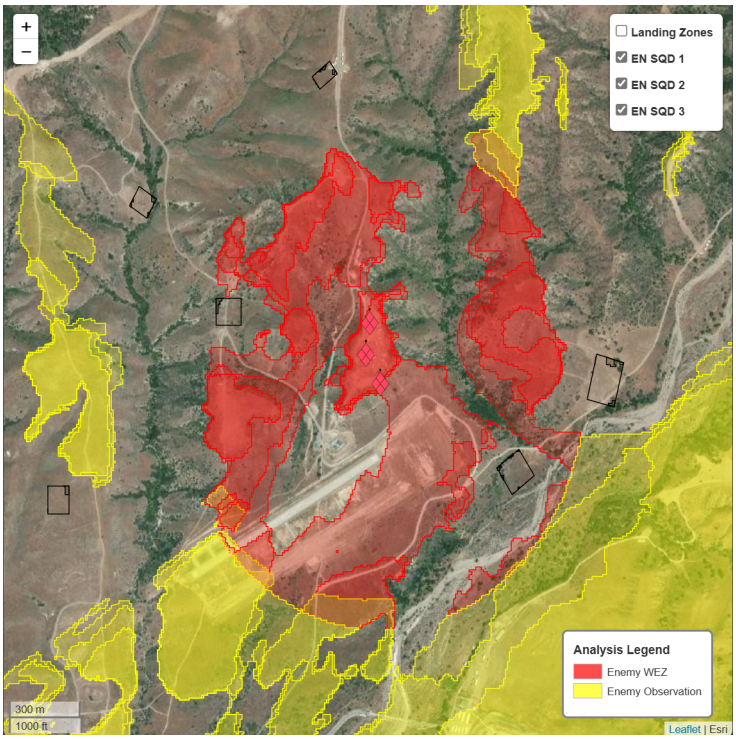

Figure 4.1. We create a subset of 6 desired HLZs from the original 192 detected. Three probable enemy infantry positions are placed on the map (red diamonds with cross). A viewshed overlay is generated and combined from these unit positions, with a target height of 6.73 meters—the height of a MV-22 Osprey. The red regions describe a direct-fire threat to a landed aircraft, while yellow regions describe enemy ability to observe a landed aircraft. After removing all HLZs not disjoint from the combined viewshed and HLZs that cannot accommodate a MV-22 section, 12 remain. We manually remove 6 HLZs within close proximity to another, eliminated redundancy.

Next, we reduce the number of possible SBF positions by filtering for minimum target distance, proximity to covered terrain, and proximity to another candidate SBF position. By removing all positions that may be closer than 300 meters to the nearest target, we ensure moderate stand-off protection from small-arms fire. Proximity to covered terrain is critical for a supporting position; the supporting unit should minimize exposure during occupation and engagement. To consider occupation exposure, the distance from every candidate SBF to the nearest limit of enemy observation or direct-fire WEZ is measured, and all positions that require more than 10 meters of exposure are removed. Lastly, we constrain candidate

SBFs for density, removing positions such that no SBF is within 40 meters of another SBF. This results in 13 candidate SBF positions for our AO (Figure 4.2).

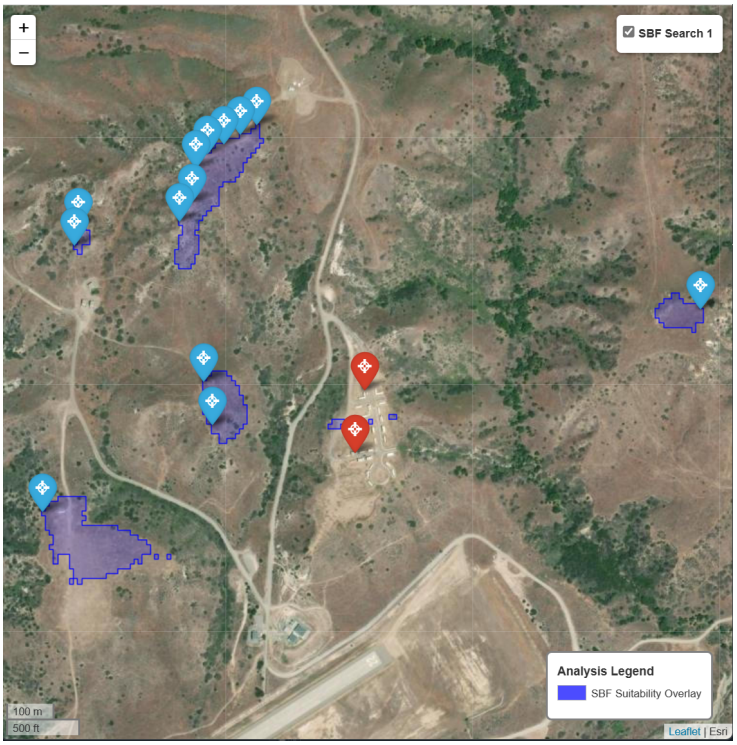

Figure 4.2. The SBF suitability overlay (blue region) delineates the 682 SBF positions that can engage both targets (red markers). We reduce the possible choices down to 13 (blue markers) by imposing three constraints. We specify that the minimum distance to target must be more than 300 meters, a covered position must be within 10 meters, and no position is within 40 meters of another choice position.

For pathfinding risk-tolerance levels, we remove the most risk-tolerant distance penalty for its likelihood to produce undesirable results. Having reduced the planning stage choices to 6 HLZs, 13 SBFs, 2 risk-tolerance levels, and 2 objective entry points, there are now 312 branch plans to evaluate. Additionally, the program pre-screens branch plans to remove any stage combinations that place the HLZ within the SDZ of the selected SBF position. This final constraint results in a manageable 220 branch plans to evaluate.

4.2 Multi-Objective Optimization for Course of Action Selection

Each of the enumerated 220 branch plan inputs (decision variable combinations) are evaluated by the objective function. The tactical pathfinding model, a multi-objective cost-path minimizer, serves as the objective function. Four decision variables are varied for each plan: the start node (HLZ), termination node (TRP), distance penalty, and SBF data layer. The SBF data layer has its own corresponding penalties—a user defined risk for crossing the MSL and the network's numeric infinity value (impassable obstacle) for the SDZ. As with the tactical pathfinding model, the minimum-cost path is quantified for each objective criteria (Table 4.1). Additional objectives are quantified for the assault phase of the maneuver (beginning after first exposure to the enemy) and the SBF selection.

Table 4.1. A table of data recorded for every COA evaluated.

Column	Description
Inputs	
Landing zone	Selected HLZ, maneuver start location
Objective entry point	Selected TRP, maneuver end location
Support by Fire	Selected SBF location
Distance penalty	Base distance cost for pathfinding risk tolerance
Outputs	
Total distance	Total maneuver distance (meters)
Total time	Total maneuver time (minutes)
Assault distance	Distance after maneuver exposure to enemy (meters)
Assault time	Time after maneuver exposure to enemy (meters)
Elevation gain	Total maneuver elevation gain (meters)
Elevation loss	Total maneuver elevation loss (meters)
Concealed distance	Total maneuver distance concealed (meters)
Unconcealed distance	Total maneuver distance unconcealed (meters)
WEZ distance	Total maneuver distance exposed to enemy field of fire (meters)
Observable distance	Total maneuver distance only observable to enemy (meters)
Roads distance	Total maneuver distance traversing known roads (meters)
Minimum target distance	Distance from SBF to closest target (meters)
Maximum target distance	Distance from SBF to furthest target (meters)
SBF cover distance	Distance from SBF to closest covered position (meters)

In the Joint Planning Process, evaluation criteria are the standards used to compare COA options relative to one another and select the best COA during COA comparison (Joint Force Development 2020). Joint Force Development (2020) provides the Weighted Numerical Comparison technique where each evaluation criteria are given an importance weight and all COAs are scored for each criteria. The weights and scores are multiplied for each criteria and summed for each COA, yielding an overall COA comparison score for each

option. Despite the formulaic process, Joint Force Development (2020) cautions "COA comparison is subjective and should not be turned into a strictly mathematical process." The Numerical Comparison technique closely reflects the weighted sum method in Multi-Objective Optimization—the technique we use to model COA evaluation and selection. For our implementation, we avoid the temptation to return a single numerically optimal solution by allowing the user to specify how many top COAs to return for subjective comparison.

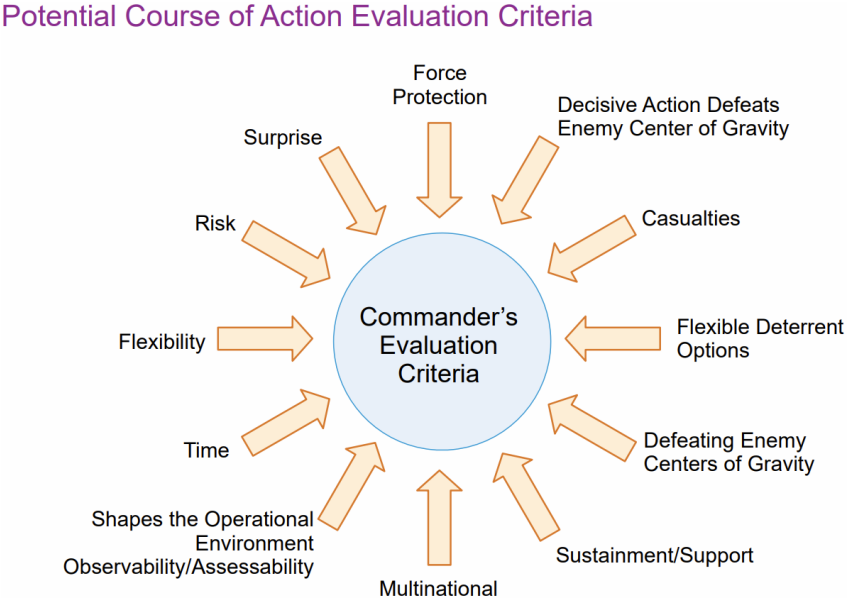

Figure 4.3. Commander's evaluation criteria is used during Step 5 of the Joint Planning Process, COA Comparison (Joint Force Development 2020). Some of these factors are not considered by our proposed models and must be accounted for by human military judgement. Other factors encompass the "art" of war—the timeless characteristics of the nature of war that also require experienced military judgement. However, components of factors such as observability, accessibility, time, risk, and surprise are quantified by our models (Table 4.1).

Index Use [~ cardinality]

$i \in I = \{1, 2, ..., m\}$	COA index [~ m COAs]
$j \in J = \{Total\ distance, total\ time, ...\}$	COA evaluation criteria [~ 14]

Given Data

n	number of COAs to select
$weight_j$	importance weight for evaluation criteria j
$evaluation_{i,j}$	normalized evaluation metric for COA i, criteria j

Decision Variables

$$X_i = \begin{cases} 1 & \text{if COA selected} \\ 0 & \text{otherwise} \end{cases}$$

Formulation

$$\min_X \quad \sum_{i=1}^{m} X_i \sum_{j=1}^{14} weight_j evaluation_{i,j}, \tag{4.1}$$

$$\text{s.t.} \quad \sum_{i=1}^{m} X_i = n, \tag{4.2}$$

$$X_i \in \{0, 1\} \qquad \forall i \in I, \tag{4.3}$$

$$\text{where,} \quad \sum_{j=1}^{14} weight_j = 1, \text{and} \quad weight_j \in [0, 1]. \tag{4.4}$$

We formulate a Multi-Objective Optimization with three data inputs: the number of COA plans the user desires to be returned, the user's importance weight for each evaluation criteria, and the evaluation criteria assessments returned by the objective function for each COA. Objective function Equation 4.1 minimizes the total weighted score of each risk evaluation criteria. Constraint 4.2 ensures that the program selects the minimum number of COAs, constraint 4.3 forces a binary selection, and constraint 4.4 ensures that all user selected weights total to 1. For our scenario, the user selected weights are listed in Table 4.2. The selected COAs are numerically described in Table 4.3 and plotted in Figure 4.4.

Table 4.2. A table of user selected evaluation criteria weights for our scenario. On this terrain, the objective is located on a finger surrounded by steep draws on three sides, so it was important to coerce solutions that avoided an axis of attack that was uphill. After elevation gain, we weighted total time, assault distance, and assault time to coerce solutions that minimized exposure to the enemy and minimized execution time.

Evaluation criteria	Selected weight
Total distance	0
Total time	0.3
Assault distance	0.1
Assault time	0.1
Elevation gain	0.5
Elevation loss	0
Concealed distance	0
Unconcealed distance	0
WEZ distance	0
Observable distance	0
Roads distance	0
Minimum target distance	0
Maximum target distance	0
SBF cover distance	0

Table 4.3. A table of COA evaluation information for the top 5 COAs selected with the multi-objective optimization model, according to weights listed in Table 4.2. Note that COA pairs 1 and 3, and 2 and 4 are the same—only with differing distance penalties. The landing zone selected was close enough to the objective that the varying risk tolerance produced negligible differences between the COAs, hence they are essentially duplicate plans in this scenario.

Selected COA	1	2	3	4	5
Stage Decisions					
Landing zone	LZ 102	LZ 102	LZ 102	LZ 102	LZ 102
Objective entry point	TRP 2	TRP 2	TRP 2	TRP 2	TRP 1
Support by Fire	SBF 304	SBF 448	SBF 304	SBF 488	SBF 78
Distance penalty	0	0	50	50	50
Evaluated Criteria					
Total distance	608.8	608.8	599.5	599.5	678.7
Total time	12.2	12.2	12.3	12.3	13.3
Assault distance	410.6	410.6	401.2	401.2	353.0
Assault time	7.8	7.8	7.8	7.8	7.1
Elevation gain	49.2	49.2	51.0	51.0	52.1
Elevation loss	-22.9	-22.9	-24.8	-24.8	-36.9
Concealed distance	0.0	0.0	0.0	0.0	0.0
Unconcealed distance	608.8	608.8	599.5	599.5	678.7
WEZ distance	399.6	399.6	393.4	393.4	172.1
Observable distance	0.0	0.0	0.0	0.0	0.0
Roads distance	19.0	9.5	18.7	9.4	19.1
Minimum target distance	321.8	657.5	321.8	657.5	568.6
Maximum target distance	389.4	701.1	389.4	701.1	739.9
SBF cover distance	8.3	0.0	8.3	0.0	0.0

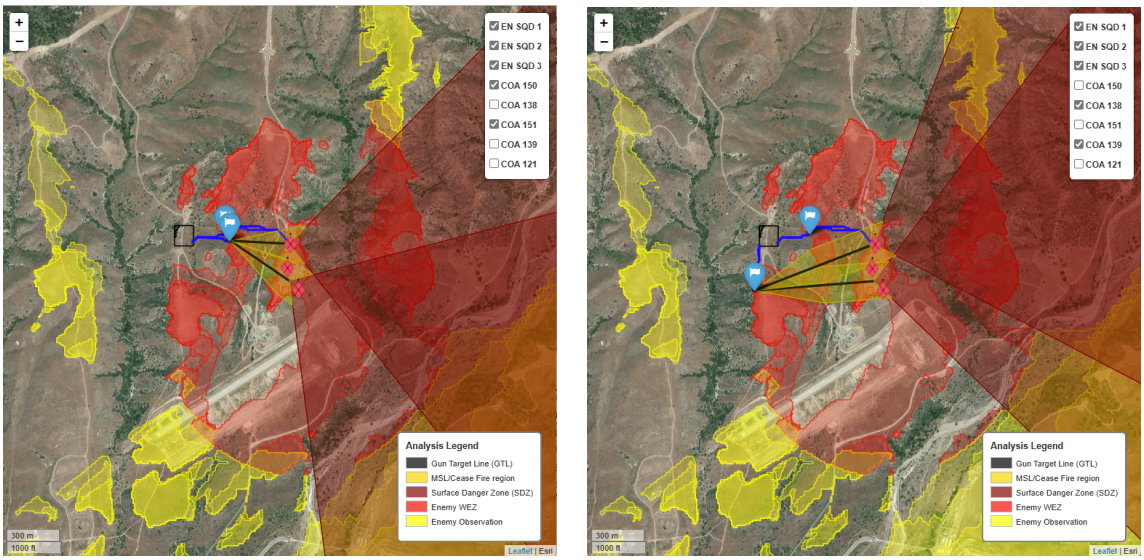

(a) COA 1 and COA 3

(b) COA 2 and COA 4

(c) COA 5

Figure 4.4. Overlays of the top 5 selected COAs from the multi-objective optimization model, selected by user criteria importance weights from Table 4.2. Note that the only variation between COA pairs in (a) and (b) is the pathfinding distance penalty, resulting in nearly identical COA pairs. Blue markers represent the closest covered position for SBFs and the assault position for maneuver routes.

4.3 Computational Efficiencies

In this section, we briefly summarize the computational efficiencies for each of the proposed models. Each process was run on a laptop with a 10th Generation Intel Core i7-10750H processor (2.60 GHz, 6 Cores, 12 Threads, 12 MB Cache) and 16 GB of DDR4 2933MHz (2 $\times$ 8 GB) memory. The processes were each run for 7 trials; the mean and standard deviations are reported in Table 4.4.

Table 4.4. Computation times for each model. A sample size of 7 runs was used to estimate means and standard deviations.

Model	Mean	Standard deviation	Remarks
HLZ generation	9.07 s	± 112 ms	1,500-meter radius, k-means
Viewshed analysis	935 ms	± 52.6 ms	3,000-meter radius, 1 unit
Tactical pathfinding	768 ms	± 18.8 ms	Dijkstra, 900-meter distance
Tactical pathfinding	784 ms	± 26.4 ms	A-star, 900-meter distance
SBF enumeration	7.51 s	± 207 ms	682 SBF positions
COA optimization	3 min 12 s	± 2.25 s	220 COAs evaluated

THIS PAGE INTENTIONALLY LEFT BLANK

CHAPTER 5: Conclusion

This thesis has provided three models that are useful to tactical-level leaders in varying scenarios: HLZ identification, tactical pathfinding, and machine gun employment. Using the output of these models to generate feasible decisions for offensive maneuvers, we provide a fourth model for COA generation and selection. Model inputs and MOEs reflect the planning and tactical thought processes used by commanders, so the results are intuitive, interpretable, and allow for human-like COA evaluation and selection. Each model individually, and especially when combined for COA generation, validates the utility in implementing data analysis for tactical planning tools. Warfare is both art and science; programs can relieve human decision-makers of the cognitive burden of deciphering the science, allowing commanders and planners to focus on the qualitative, human, and intangible aspects of warfare.

5.1 Implementation

Research sponsors have provided funding and labor to develop an ATAK plug-in to make our models widely available to the force. The plug-in will enable model utilization on any fielded or personal Android device. A port to WinTAK-MIL will allow for model use on any Windows machine and testing on edge computing platforms such as the ICOP. Several infantry battalions and training groups are prepared to test and implement the application.

5.2 Future Work

We categorize possibilities for future work as improvements, extensions, or applications. Model improvements listed will generally result in decreased input sensitivity, while extensions add to the mission set for which this capability may be used. Model applications discussed are generally more abstract uses of the models for follow-on research.

5.2.1 Model Improvements

There are several areas in which the robustness and utility of our models may be improved. Beginning with the HLZ model, we have implemented a fairly basic algorithm to determine the number of cluster labels to use when dividing a suitable HLS polygon. This algorithm does not account for the relative size or geometry of the region. Once sufficiently trained, a neural network may be an effective tool to transform the binary HLS raster into a single integer representing the ideal number of clusters for that suitability region.

In the tactical pathfinding model, the user must use default profiles or manually adjust the risk weights for the terrain assessment. In some scenarios, this may require a trial-and-error process to select weights that return sufficiently unique solutions. A more robust implementation may be achieved with the application of a Pareto front to select weights and return efficient solutions.

5.2.2 Model Extensions

Several extensions to the models may expand applicable use-cases and result robustness. For offensive maneuvers, we can extend our COA generation model to include the selection of indirect fire positions and final attack headings for close air support. A linear program could deconflict these assets laterally, by altitude, or by time when scheduling fires.

Similarly to offensive maneuvers, we may implement a model for defensive operations. The selection of defensive positions and employment of weapons and anti-armor assets while maximizing blocking capability and coverage of dead space is a process that could be similarly optimized. With the implementation of both models, attacker-defender modeling could yield interesting research and allow unit-leaders to war-game their own operations.

Our model uses deterministic locations for enemy positions. Naturally, this means that the model can be very sensitive to the resulting viewsheds built from these enemy positions. Reduced sensitivity and increased robustness may be achieved my implementing a stochastic model for probable enemy locations based on the last known observation.

5.2.3 Model Applications

The pathfinding and HLZ models are being applied in support of future unmanned aerial logistics vehicles. Reconfigurable and autonomous resupply vehicles will greatly improve the sustainability of forces persisting within the WEZ in EABs. These systems will also require network-based decision support tools for generating minimum-cost flows for troop resupply.

Adjusting the parameters of the HLZ model also allows for the discretized enumeration of firing points for ground-based anti-ship missile (GBASM) capabilities. This is inherently useful for special operations, reconnaissance units, and conventional Stand-In forces as an operational planning tool. Furthermore, it provides the basis for analysis and decision aids regarding the survivability and employment of firing systems and their respective supply points and operation centers in the First and Second Island Chains.

Recent achievements have been made regarding the success of artificially intelligent agents defeating world-class human players in real-time strategy games. These games have similar characteristics to warfare in that decisions must be made with imperfect or incomplete information, without immediate feedback, and have long-term payoff or consequences. Neural networks that train multi-agent systems to play these games require a lever mechanism to interact and make decisions in the game. The offensive COA model generated in this thesis could be foundational to act as such a lever for a system trained in simulation or by data collected from real forces.

THIS PAGE INTENTIONALLY LEFT BLANK

APPENDIX: Additional Results

A.1 Additional Helicopter Landing Zone Regions

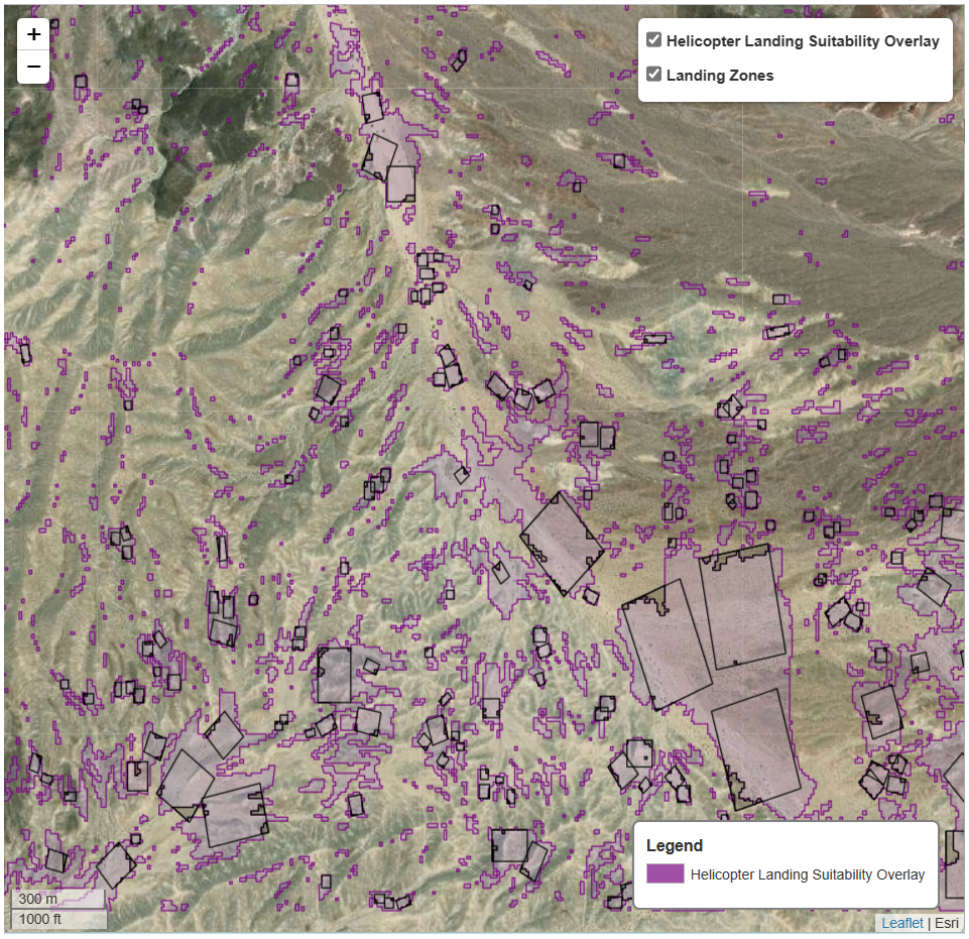

Figure A.1. HLZ search results in Twentynine Palms, California. HLS regions are represented in purple and viable HLZs are represented by black landing boxes. For a slope threshold of 2.5 degrees, the model yielded a HLS utilization of 34.69%.

Figure A.2. HLZ search results in Quantico, Virginia. HLS regions are represented in purple and viable HLZs are represented by black landing boxes. For a slope threshold of 3 degrees, the model yielded a HLS utilization of 30.44%.

A.2 Additional Course of Action Generation Scenario

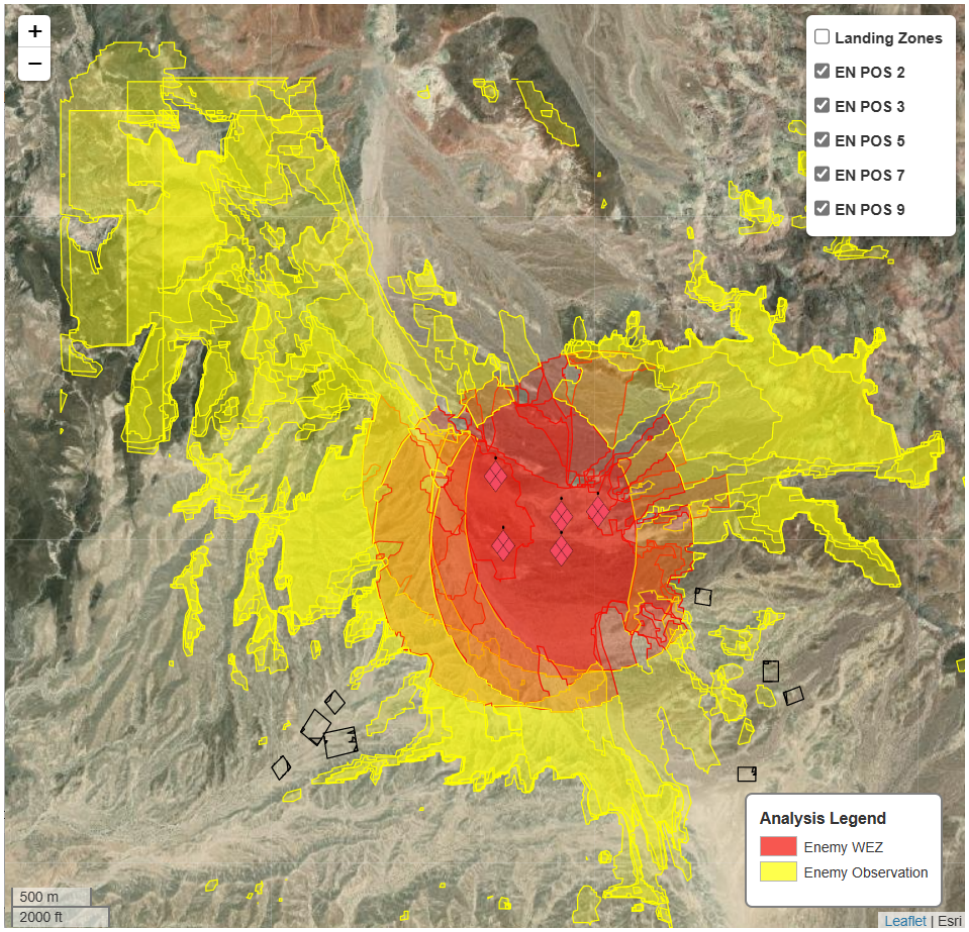

Figure A.3. HLZ search options that are covered from enemy direct-fire and observation for the Regimental Assault Course (executed by the Tactical Training and Exercise Control Group). Enemy battle positions are represented by red diamonds with a black cross, red regions represent areas within a 1,000-meter WEZ of each position, and yellow regions represent observable areas outside of the WEZ. HLZ options are given by black boxes.

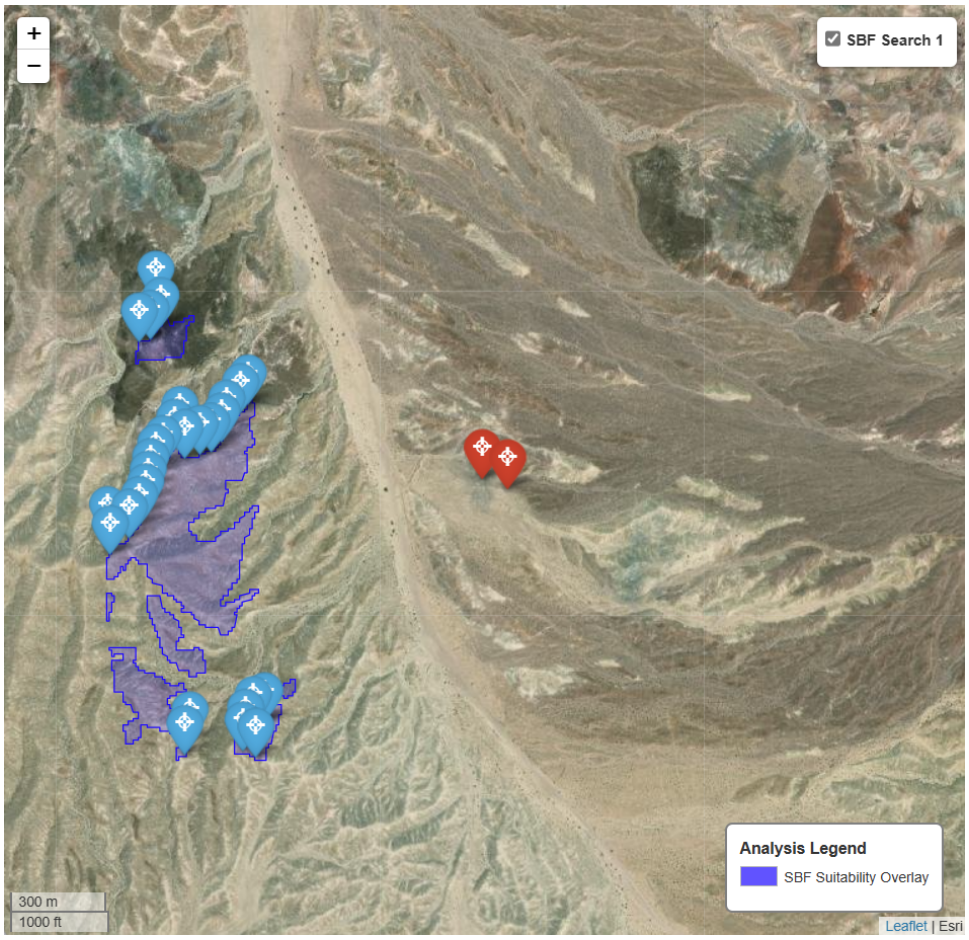

Figure A.4. SBF options for the employment of medium machine guns during the Regimental Assault Course (executed by the Tactical Training and Exercise Control Group). The blue regions represent the area of viable positions from which an M240G can effect both targets (red markers) simultaneously. Blue markers are SBF positions that have cover available within 10 meters.

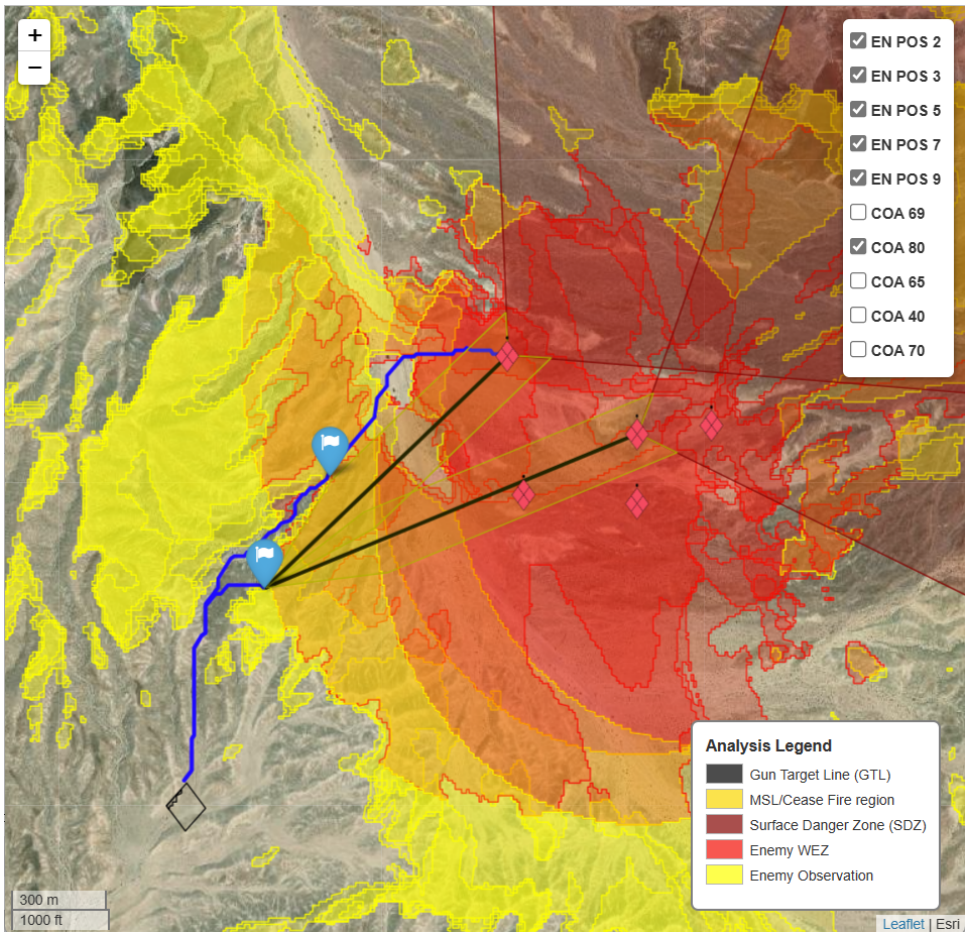

Figure A.5. An optimal COA generated for the execution of the Regimental Assault Course (executed by the Tactical Training and Exercise Control Group). Black lines represent the SBF gun-target lines, dark yellow regions represent the associated MSLs, and dark red regions represent the SDZs. Blue lines represent routes to the objective and SBF position. The blue markers represent the covered position for SBF and the assault position for the maneuvering unit.

THIS PAGE INTENTIONALLY LEFT BLANK

List of References

Air Force Research Laboratory (n.d.) Tactical Assault Kit (TAK) – Air Force Research Laboratory. URL https://afresearchlab.com/technology/information-technology/tactical-assault-kit-tak/.

Berger D (2019) *38th Commandant's Planning Guidance*. Marine Corps Publications Electronic Library, Quantico, VA, URL https://www.marines.mil/News/Publications/MCPEL/Electronic-Library-Display/Article/1907265/38th-commandants-planning-guidance-cpg/.

Brose C (2020) *The Kill Chain: Defending America in the Future of High-Tech Warfare* (Hachette Books), ISBN 978-0-316-53353-9, URL https://books.google.com/books?id=cQVUyAEACAAJ.

Department of the Army (2014) *Range Safety*. DA-PAM 385-63, Washington, DC, URL https://www.marines.mil/News/Publications/MCPEL/Electronic-Library-Display/Article/1170774/da-pam-385-63/.

Erskine J, Oxendine C, Wright W, O'banion M, Philips A (2022) Evaluating the relationship between data resolution and the accuracy of identified helicopter landing zones (HLZs). *Applied Geography* 139:102652, ISSN 0143-6228, URL http://dx.doi.org/https://doi.org/10.1016/j.apgeog.2022.102652.

ESA WorldCover (n.d.) About WorldCover. URL https://esa-worldcover.org/en/about/about.

Esri (n.d.) Creating a cost surface raster—ArcGIS Pro | Documentation. URL https://pro.arcgis.com/en/pro-app/latest/tool-reference/spatial-analyst/creating-a-cost-surface-raster.htm.

Google Developers (n.d.) API Reference Google Earth Engine. URL https://developers.google.com/earth-engine/apidocs.

Google Earth Engine (n.d.) Earth Engine Data Catalog. URL https://developers.google.com/earth-engine/datasets.

Hanaki S (2022) PMW 120 Overview. URL https://www.ndia-sd.org/wp-content/uploads/Briefs/Fall2022/NDIA_Fall_Forum_PMW_120_2022.pdf.

Headquarters, Marine Corps (2015a) *Geospatial Information and Intelligence*. MCRP 2-10B.4, Quantico, VA, https://www.marines.mil/News/Publications/MCPEL/Electronic-Library-Display/Article/900520/mcrp-2-10b4-formerly-mcwp-2-26/.

Headquarters, Marine Corps (2015b) *Marine Corps Planning Process*. MCWP 5-10, Quantico, VA, URL https://www.marines.mil/News/Publications/MCPEL/Electronic-Library-Display/Article/900553/mcwp-5-10/.

Headquarters, Marine Corps (2018a) *Commander's Tactical Handbook*. MCRP 3-30.7, Quantico, VA, URL https://www.marines.mil/News/Publications/MCPEL/Electronic-Library-Display/Article/899844/mcrp-3-307-formerly-mcrp-3-111a/.

Headquarters, Marine Corps (2018b) *Intelligence Operations*. MCWP 2-10, Quantico, VA, URL https://www.marines.mil/News/Publications/MCPEL/Electronic-Library-Display/Article/899569/mcwp-2-10/.

Headquarters, Marine Corps (2019) *Air Assault Operations*. MCTP 3-01B, Quantico, VA, URL https://www.marines.mil/News/Publications/MCPEL/Electronic-Library-Display/Article/1791144/mctp-3-01b/.

Headquarters, Marine Corps (2021) *Machine Guns and Machine Gunnery*. MCTP 3-01C, Quantico, VA, URL https://www.marines.mil/News/Publications/MCPEL/Electronic-Library-Display/Article/900523/mctp-3-01c/.

Joint Force Development (2020) *Joint Planning*. JP 5-0, Washington, DC, URL https://www.jcs.mil/Doctrine/Joint-Doctrine-Pubs/5-0-Planning-Series/.

Jong D, Kwon I, Goo D, Lee D (2015) Safe pathfinding using abstract hierarchical graph and influence map. 860–865, URL http://dx.doi.org/10.1109/ICTAI.2015.125.

Kang MW, Jha M, Hwong D (2011) A GIS-based simulation model for military path planning of unmanned ground robots. *International journal of safety and security engineering* 1(3):248–264, ISSN 2041-9031.

Kovarik V, Rybansky M (2014) Selecting locations for landing of various formations of helicopters using spatial modelling. *IOP Conference Series: Earth and Environmental Science* 18, URL http://dx.doi.org/10.1088/1755-1315/18/1/012132.

Magyari-Sáska Z, Dombay S (2012) Determining minimum hiking time using DEM. *Geographica Napocensis Anul* 82(4):124–129.

National Geospatial-Intelligence Agency (2019) NGA Standardization Document - Digital Elevation Content Standardization Implementation Guidance.

Piedfort M (2022) NIWC Pacific's all-source Intelligence Carry On Program reimagines DevSecOps for the fleet. *CHIPS* URL https://www.doncio.navy.mil/chips/ArticleDetails.aspx?ID=15728.

Pokonieczny K (2018) Use of a multilayer perceptron to automate terrain assessment for the needs of the armed forces. *ISPRS International Journal of Geo-Information* 7(11):430, ISSN 2220-9964, URL http://dx.doi.org/10.3390/ijgi7110430.

Pokonieczny K, Wyszynski M (2016) Automation of the terrain assessment classification due to passability for the needs of crisis management. URL http://dx.doi.org/10.5593/SGEM2016/B23/S11.016.

TAK Product Center (n.d.) Android Team Awareness Kit or ATAK / CivTAK. URL https://www.civtak.org/atak-about/.

The Basic School, Marine Corps Training Command (n.d.) *Machine Gun Employment Student Handout*. B3N0511XQ-DM, Camp Barrett, VA, URL https://www.trngcmd.marines.mil/Portals/207/Docs/TBS/B3N0511XQ-DM%20Machine%20Gun%20Employment.pdf.

Tollefson B (2021) Intelligence, Surveillance, Reconnaissance and Information Operations. URL https://www.niwcpacific.navy.mil/isr-io/.

US Census Bureau (2016) TECHNICAL DOCUMENTATION: 2016 TIGER/Line Shapefiles. URL https://www2.census.gov/geo/pdfs/maps-data/data/tiger/tgrshp2016/TGRSHP2016_TechDoc.pdf.

US Census Bureau (2016) TIGER/Line Geodatabases. URL https://www.census.gov/geographies/mapping-files/time-series/geo/tiger-geodatabase-file.html, section: Government.

US Geological Survey (2020) 1/3rd arc-second Digital Elevation Models (DEMs) - USGS National Map 3DEP Downloadable Data Collection: U.S. Geological Survey. URL https://www.sciencebase.gov/catalog/item/4f70aa9fe4b058caae3f8de5.

Zanaga D, Van De Kerchove R, De Keersmaecker W, Souverijns N, Brockmann C, Quast R, Wevers J, Grosu A, Paccini A, Vergnaud S, Cartus O, Santoro M, Fritz S, Georgieva I, Lesiv M, Carter S, Herold M, Li L, Tsendbazar NE, Ramoino F, Arino O (2021) ESA WorldCover 10 m 2020 v100. URL http://dx.doi.org/10.5281/zenodo.5571936.

THIS PAGE INTENTIONALLY LEFT BLANK

Initial Distribution List

1. Defense Technical Information Center
   Ft. Belvoir, Virginia

2. Dudley Knox Library
   Naval Postgraduate School
   Monterey, California